TKK Dissertations 170
Espoo 2009

# CONFORMATIONS AND DYNAMICS OF STRONGLY CHARGED BIOMOLECULES

Doctoral Dissertation

**Olli Punkkinen**

**Helsinki University of Technology**
**Faculty of Information and Natural Sciences**
**Department of Applied Physics**

TKK Dissertations 170
Espoo 2009

# CONFORMATIONS AND DYNAMICS OF STRONGLY CHARGED BIOMOLECULES

Doctoral Dissertation

**Olli Punkkinen**

Dissertation for the degree of Doctor of Science in Technology to be presented with due permission of the Faculty of Information and Natural Sciences for public examination and debate in Auditorium E at Helsinki University of Technology (Espoo, Finland) on the 4th of June, 2009, at 12 noon.

**Helsinki University of Technology**
**Faculty of Information and Natural Sciences**
**Department of Applied Physics**

**Teknillinen korkeakoulu**
**Informaatio- ja luonnontieteiden tiedekunta**
**Teknillisen fysiikan laitos**

Distribution:
Helsinki University of Technology
Faculty of Information and Natural Sciences
Department of Applied Physics
P.O. Box 1100 (Otakaari 1M)
FI - 02015 TKK
FINLAND
URL: http://tfy.tkk.fi/
Tel.  +358-9-451 3101
E-mail: Eija.Jarvinen@tkk.fi



ISBN 978-951-22-9915-7
ISBN 978-951-22-9917-1 (PDF)
ISSN 1795-2239
ISSN 1795-4584 (PDF)
URL: http://lib.tkk.fi/Diss/2009/isbn9789512299171/

TKK-DISS-2614

Multiprint Oy
Espoo 2009

| ABSTRACT OF DOCTORAL DISSERTATION | HELSINKI UNIVERSITY OF TECHNOLOGY<br>P. O. BOX 1000, FI-02015 TKK<br>http://www.tkk.fi |
|---|---|

Author Olli Punkkinen

Name of the dissertation

Conformations and Dynamics of Strongly Charged Biomolecules


| | |
|---|---|
| Manuscript submitted 10.3.2009 | Manuscript revised |
| Date of the defence 4.6.2009 (tentative) | |
| ☐ Monograph | ☒ Article dissertation (summary + original articles) |

| | |
|---|---|
| Faculty | Faculty of Information and Natural Sciences |
| Department | Department of Applied Physics |
| Field of research | Biological Physics |
| Opponent(s) | Prof. Ralf Metzler |
| Supervisor | Prof. Tapio Ala-Nissilä |
| Instructor | Prof. Ilpo Vattulainen and Prof. Rudolf Podgornik |



Abstract

This Thesis is based on analytical and numerical calculations concerning strongly charged biomolecules. The study concentrates on statistical properties of strongly charged biopolymers in the presence of neutralizing counterions and reservoir salt ions, involving applications on deoxyribonucleic acid (DNA), which is a key molecule in human cells. The Thesis starts from constructing a theory that explains the counter- and coion distributions around an arbitrary strongly charged surface, and moves to applications involving statistical conformations of highly stretched DNA, and dynamics of settling the DNA chain in the presence of a large amount of reservoir salt.

Studies on ion-distributions around a charged surface concentrate on finding a theoretical description in the limit where electrostatic interactions between the ions and the charged surface are so strong that they dominate over the translational entropy of the counter- and coions. In particular we explain how the added electrolyte or salt modifies the ion distributions compared to the zero salt case, a topic which is highly relevant for bioapplications that take place under physiological salt concentration.

Application on the DNA overstretching transition involves the evaluation of the response of the chain to a strong external stretching force. Here we explain how the force needed to extend the chain depends on the added electrolyte concentration. We concentrate on finding the conformation of the chain over the persistence length of DNA, and the equation of state for DNA as a function of the stretching force.

Studies on dynamical properties of DNA concern the sedimentation velocity of a long DNA chain under physiological salt conditions that it is typically described using the self-avoiding walk (SAW) model. Here we show that in the limit of large polymer or Reynolds number, the chain goes through a crossover in its shape, transforming from slightly perturbed SAW chain into an elongated configuration along the direction of sedimentation. We present a model that couples the instant configuration in a non-linear way to the settling velocity of the chain. This way the scaling laws for both the radius of gyration of the chain characterizing its size, and for the diffusion coefficient of the chain characterizing its dynamics, are found to be in agreement with numerical simulations.



| | |
|---|---|
| Keywords Strong Coupling, Overcharging, Overstretching, Sedimentation | |
| ISBN (printed) 978-951-22-9915-7 | ISSN (printed) 1795-2239 |
| ISBN (pdf) 978-951-22-9917-1 | ISSN (pdf) 1795-4584 |
| Language English | Number of pages 108p. + app. 42p. |
| Publisher Department of Applied Physics, Helsinki University of Technology | |
| Print distribution Department of Applied Physics, Helsinki University of Techology | |
| ☒ The dissertation can be read at http://lib.tkk.fi/Diss/2009/isbn9789512299171/ | |

| VÄITÖSKIRJAN TIIVISTELMÄ | TEKNILLINEN KORKEAKOULU<br>PL 1000, 02015 TKK<br>http://www.tkk.fi |
|---|---|

Tekijä Olli Punkkinen

Väitöskirjan nimi

Voimakkaasti varattujen biomoolekyylien tasapainomuodot ja dynamiikka

| Käsikirjoituksen päivämäärä 10.3.2009 | Korjatun käsikirjoituksen päivämäärä |
|---|---|

Väitöstilaisuuden ajankohta 4.6.2009

| ☐ Monografia | ☒ Yhdistelmäväitöskirja (yhteenveto + erillisartikkelit) |
|---|---|

| | |
|---|---|
| Tiedekunta | Informaatiotekniikan ja Luonnontieteiden Tiedekunta |
| Laitos | Teknillisen fysiikan laitos |
| Tutkimusala | Biologinen fysiikka |
| Vastaväittäjä(t) | Prof. Ralf Metzler |
| Työn valvoja | Prof. Tapio Ala-Nissilä |
| Työn ohjaaja | Prof. Ilpo Vattulainen ja Prof. Rudolf Podgornik |


Tiivistelmä

Tämä väitöskirja perustuu voimakkaasti varattujen biomolekyylien teoreettiseen ja numeeriseen tutkimukseen. Väitöstutkimus käsittelee biomolekyylien elektrostaattisia ominaisuuksia, perustuen kanonisten tasapainojakaumien laskemiseen, ja sitä kautta biomolekyylien fysikaalisten ominaisuuksien määrittämiseen. Erityisesti olemme kiinnostuneita siitä, miten DNA:ta ympäröivien suolaionien konsentraatio vaikuttaa DNA:n tasapainotilaan. Väitöskirjan ensimmäinen puolisko, eli Artikkelit I ja II käsittelevät varattuja biomolekyylejä ympäröivien ionien tasapainojakauman laskemista niin sanotun vahvan elektrostaattisen kytkennän rajalla. Väitöskirjan jälkimmäinen puolisko sen sijaan käsittelee DNA:ta koskevia sovelluksia, kuten DNA:n tilanyhtälöa ulkoisen venyttävän voiman funktiona Artikkelissa III, sekä biopolymeerien kuten DNA:n sedimentaatiota suolaliuoksessa Artikkelissa IV.

Voimakkaasti varattujen molekyylien teoriassa olemme tutkineet sitä, miten ympäröivän nesteen suolakonsentraatio vaikuttaa ionien jakaumaan tutkittavan varatun makromolekyylin ympärillä. Tutkimusaihe on hyvin kiinnostava biologisen fysiikan sovelluksissa, joissa varatut biomolekyylit ovat fysiologisessa suolaliuoksessa.

DNA-molekyylin ylivenymätransitio puolestaan on kiinnostava esimerkiksi tutkittaessa DNA-transkriptiota. Tässä tutkimuksessa olemme määrittäneet DNA:n tilanyhtälöä ulkoisen venyttävän voiman funktiona, ja ylivenymätransitioon tarvittavaa voimaa ympäröivan suolaliuoksen funktiona. Merkittävin tulos kyseisessä työssä on se, että suolariippuvuus saadaan yhteneväiseksi kokeellisten tulosten kanssa, ja se riippuu ainoastaan varausten efektiivisestä etäisyydestä DNA-molekyyliä pitkin.

Polymeerien sedimentaatiota koskeva osa väitöskirjaa käsittelee biopolymeerien kuten DNA:n sedimentaationopeuden ja sedimentaatiokonformaation riippuvuutta DNA:n koosta eli monomeerien lukumäärästä. Oletuksena teoriassa on se, että tutkittava näyte sisältää riittävästi suolaa, jotta polymeerille voidaan käyttää ns. itseään välttelevän ketjun approksimaatiota. Esittämämme teoria kytkee epälineaarisella tavalla polymeerin hetkellisen konformaation vaikutuksen polymeerin sedimentaationopeuteen. Teorian ennustamat skaalausargumentit polymeerin gyraatiosäteelle ja diffuusiokertoimelle ovat sopusoinnussa simulaatiotulosten kanssa.



Asiasanat Voimakas kytkentä, Ylivarautuminen, denaturoituminen, sedimentaatio

| ISBN (painettu) 978-951-22-9915-7 | ISSN (painettu) 1795-2239 |
|---|---|
| ISBN (pdf) 978-951-22-9917-1 | ISSN (pdf) 1795-4584 |
| Kieli Englanti | Sivumäärä 108s. + liit. 42s. |

Julkaisija Teknillisen fysiikan laitos

Painetun väitöskirjan jakelu Teknillisen fysiikan laitos

☒ Luettavissa verkossa osoitteessa http://lib.tkk.fi/Diss/2009/isbn9789512299171/

# Preface

The work reported in this Thesis has been carried out while working at the Laboratory of Physics and Helsinki Institute of Physics at Helsinki University of Helsinki. I want to thank my instructor and boss, Professor Ilpo Vattulainen for giving me a chance to work at his group, Biological and Soft Matter Group at the Department of Physics. Ilpo has always couraged me during these years to continue and finnish the work I have started. My supervisor, Professor Tapio Ala-Nissilä has been supportive towards my crazy theoretical ideas, thanks for that, I think it has paid back. Next I want to thank my instructor Professor Rudolf Podgornik for quiding me in this work, essentially in helping me to *see the physics* from my theoretical derivations. Also, thanks are deserved by my previous instructor Assistant professor Per-Lyngs Hansen, who always made me feel that I have really done something important. I want to thank also my group members, and my room mates who have been willing to help me and quide me countless times. Next I want to thank my parents Matti and Pirkko-Liisa, and my mother-in-law Päivi, who made it possible for me to finnish this Thesis. Your help, especially in taking care of my little Son Valtteri, has been invaluable. To be honest, I don't know how to thank you enough. Special thanks are deserved by my father Matti, who made me enthusiasted about solving scientific problems, and has always believed that I have a talent to work them out. My mother Pirkko-Liisa has been very supportive towards me through my whole life, and she has convinced me that I can manage whatever I'm up to. Finally, I want to thank my dear wife Henna, who has always been there for me understanding my impatience and carrying me through difficult times of my life. I guess I have not told you this too often, but I think I would have not survived all these years without You. Also, you have given me a great son Valtteri, whose endless etnthusiasm just about everything has given me patience and energy to finish the work presented in this Thesis.

# Contents

# List of Publications

This thesis consists of an overview and of the following publications which are referred to in the text by their Roman numerals.

**I** O. Punkkinen, A. Naji, R. Podgornik, I. Vattulainen, and P. L. Hansen, "*Ionic Cloud Distribution Close to a Charged Surface in the Presence of Salt*", Europhysics Letters **82**, 48001 (2008).

**II** O. Punkkinen, A. Naji, I. Vattulainen, and R. Podgornik, "*Counter- and Coion Distributions Close to a Strongly Charged Surface in the Limit of Weakly Coupled Bulk Salt*", HIP-2009-12/TH

**III** O. Punkkinen, P. L. Hansen, L. Miao, and I. Vattulainen, "*DNA Overstretching Transition: Ionic Strength Effects*", Biophys. J. **89**, 967 (2005).

**IV** V. Lehtola, O. Punkkinen, and T. Ala-Nissila, "*Polymer Scaling and Dynamics in Steady-State Flow*", Phys. Rev. E **76**, 051802 (2007).

# Author's contribution

The author has played an active role in all stages of the research reported in this Thesis.

Publications I and II were authored together with Ilpo Vattulainen, Ali Naji, Rudolf Podgornik and Per-Lyngs Hansen. The author planned and executed completely the work described in publications I and II. He developed the model, calculated analytically the ion-densities, wrote the numerical solver for the ion-densities, and analyzed the data. The author also wrote the first draft of both publications.

Publication III was authored together with Ling Miao, Per-Lyngs Hansen and Ilpo Vattulainen. The author developed the theoretical model and also calculated the analytical results, wrote the analysis tools, and wrote the first draft of the publication.

Publication IV was authored together with Ville Lehtola and Tapio Ala-Nissilä. The author planned the theoretical model to explain the simulation data. The author also actively took part in the planning of simulations, but the simulations were carried out by Ville Lehtola. The author wrote the parts describing the theory into the first draft of the publication.

Additional publications of the author (not included in this Thesis):

- O. Punkkinen, E. Falck, and I. Vattulainen, *Dynamics and Scaling of Polymers in a Dilute Solution: Analytical Treatment in Two and Higher Dimensions*, J. Chem. Phys. **122**, 094904 (2005).
- E. Falck, O. Punkkinen, I. Vattulainen, and T. Ala-Nissila, *Dynamics and Scaling of 2D Polymers in a Dilute Solution*, Phys. Rev. E Rapid Comm. **68**, 050102 (2003).

- J. Punkkinen, I. Konkka, O. Punkkinen, T. Korpi-Tommola, M. Färkkilä, and J. Koskenpato, *Measuring Gastric Emptying:Comparison of Octanoic Acid Breath and Scintigraphy*, Digestive Diseases and Sciences, **51**, 262 (2006).

# List of Abbreviations

| | |
|---|---|
| SC | Strong Coupling |
| DH | Debye-Hückel |
| SCWDH | Strong Coupling with Debye-Hückel |
| PB | Poisson-Boltzmann |
| OC | Overcharging |
| GC | Gouy-Chapman |
| WLC | Wormlike Chain |
| ss | Single stranded |
| ds | Double stranded |
| CM | Center of Mass |
| NS | Navier-Stokes |
| HI | Hydrodynamic Interaction |
| SAW | Self-avoiding Walk |

# List of Symbols

| | |
|---|---|
| $\phi$ | Fluctuating Electrostatic Field |
| $\mathcal{H}$ | Hamiltonian |
| $\epsilon$ | Dielectric constant |
| $e$ | Unit Electric Charge |
| $\mu$ | Gouy-Chapman Length |
| $l_B$ | Bjerrum Length |
| $\kappa$ | Debye Screening Parameter |
| $l_{DH}$ | Debye Screening Length |
| $\mathbf{r}$ | Position Vector |
| $\mathbf{k}$ | Wave Vector |
| $\sigma_s$ | Surface Charge Density |
| $\sigma(\mathbf{r})$ | External Charge Density |
| $q_c$ | Valence of Counterions |
| $q_+$ | Valence of Positive Salt Ions |
| $q_-$ | Valence of Negative Salt Ions |
| $k_BT$ | Thermal Energy |
| $\beta$ | Inverse Thermal Energy |
| $a$ | Radius of Ion |
| $\rho_\alpha(\mathbf{r})$ | Density of Ion-type $\alpha$ |
| $Q_{int}(z)$ | Integrated Charge / Apparent Surface Charge |
| $N$ | Number of Monomers in Polymer Chain |
| $\rho(\mathbf{r})$ | Perpendicular Fluctuation of the Chain Coordinate |
| $u_z(z)$ | Stretching Field |
| $b$ | Microscopic Cutoff Distance |
| $a_0$ | Structural Separation between Monomers along Polymer Chain |
| $c$ | Renormalized Separation between Charges along DNA |
| $\lambda$ | Stretching Modulus |
| $\lambda^{(R)}$ | Renormalized Stretching Modulus |
| $K_C$ | Bending Modulus |

| | |
|---|---|
| $K_C^{(R)}$ | Renormalized Bending Modulus |
| $L_0$ | Structural Length of DNA |
| $L$ | Legth of Stretched DNA |
| $f$ | External Stretching Force |
| $x$ | Extension of Chain in Direction of $f$ |
| $\sigma_i$ | Ising-variable |
| $H$ | Ising Parameter for External Field |
| $J$ | Ising Parameter for Nearest-neighbour Interaction |
| $\delta$ | Relative Elongation of S-DNA compared to B-DNA |
| $g(f)$ | Free Energy Density of Elastic Chain |
| $\Delta$ | Stretching Parameter |
| $\eta$ | Viscosity of Solvent |
| $\rho$ | Density of Solvent |
| $Re$ | Reynolds Number |
| $g$ | Gravitational Constant |
| $\mathbf{v}(\mathbf{r})$ | Three-dimensional Velocity Field |
| $\mathbf{r}_n$ | Position Vector of n$^{th}$ monomer |
| $\mathbf{H}(\mathbf{r}-\mathbf{r}')$ | Oseen-Tensor |
| $\mathbf{H}(n-m)$ | Pre-averaged Oseen Tensor between Monomers $n$ and $m$ |
| $\mathbf{v}_{CM}$ | Velocity of Center of Mass of Polymer |
| $\delta\mathbf{v}_{CM}$ | Velocity Fluctuation of Center of Mass of Polymer |
| $\mathbf{v}_{lim}$ | Ensemble Average of Velocity of CM in Direction of Sedimentation |
| $\mathbf{P}$ | CM of Momentum |
| $\mathbf{p}_n$ | Momentum of n$^{th}$ Monomer |
| $\mathbf{f}_n$ | Force Acting on n$^{th}$ Monomer |
| $R_G$ | Radius of Gyration |
| $R_{G,\parallel}$ | Radius of Gyration in Direction of Sedimentation |
| $R_{G,\perp}$ | Radius of Gyration in Perpendicular Direction to Sedimentation |
| $D$ | Diffusion Coefficient |
| $\nu$ | Scaling Exponent of Radius of Gyration |

| | |
|---|---|
| $\nu_{\parallel}$ | Scaling Exponent of Radius of Gyration in Direction of Sedimentation |
| $\nu_{\parallel}$ | Scaling Exponent of Radius of Gyration in Direction Perpendicular to Sedimentation |
| $\nu_D$ | Scaling Exponent of CM Diffusion Coefficient |
| $\nu_{D,\parallel}$ | Scaling Exponent of CM Diffusion Coefficient in Direction of Sedimentation |
| $\nu_{D,\perp}$ | Scaling Exponent of CM Diffusion Coefficient in Direction Perpendicular to Sedimentation |
| $N_{head}$ | Number of Monomers in Head Part of a Polymer |
| $N_{tail}$ | Number of Monomers in Tail Part of a Polymer |
| $\alpha$ | $R_{\perp}/R_{\parallel}$ |
| $U(\{\mathbf{r}_n\})$ | Interaction Potential of a Polymer Chain |

# 1 Introduction

In this Thesis, we consider a topic that is very interesting in many daily applications, that is electric charges. This belongs to the branch of science called electrostatics, which deals with stationary or very slowly moving charges, and how it affects the physical properties of various biomolecules we encounter in the human body [25].

Historically it has been known that some materials such as amber emit light particles after rubbing. More familiarly, everyone of us knows that while rubbing dry hair with a comb, individual strands of hair tend to rise up and straighten slightly. This is an example of static electricity that is produced by the comb into the hair. By rubbing the hair one makes electrons to move from the hair into the comb, leaving a surplus of positive charge carriers into the hair. This creates a repulsive force between the positively charged strandes of hair, causing them to move apart from each other by straightening and rising up. In the same way, amber becomes negatively charged after rubbing.

Other familiar electrostatic phenomena include many simple examples such as the attraction of plastic wrap to one's hand after one removes it from a package, the apparently spontaneous explosion of grain silos, damage of electronic components during manufacturing and the operation of photocopiers. More generally, electrostatic phenomena arise from the forces that electric charges exert on each other, namely the Coulombic forces. Even though electrostatically induced forces seem to be rather weak, the electrostatic force between an electron and a proton that together make up the hydrogen atom, is about 40 orders of magnitude stronger than the gravitational force acting between them.

Yet another example from daily life is milk, which people in western countries drink every day. Milk is an emulsion of water-based fluid and butterfat colloid, which carry an electrical charge. Each fat globule in milk is surrounded by a membrane consisting of phospholipids and proteins that keep the individual globules from joining together into

large grains of butterfat and also protects the globules from the fat-digesting activity of enzymes found in the fluid portion of milk. The largest structures in the fluid portion of milk are casein protein micelles, which are aggregates of several thousand protein molecules bonded together by calcium phosphate. The outermost layer of these micelles consists of strands of one type of protein, Kappa-casein, reaching out from the body of the micelle into the surrounding fluid. These Kappa-casein molecules have a negative electrical charge and therefore repel each other, keeping the micelles separated under normal conditions and thus stabilizing this colloidal suspension in milk [44].

All the examples presented above demonstrate the phenomenon that most of scientist consider as self-evident, namely that similarly charged objects repel each other, and oppositely charged objects attract each other. Thus, it was a major surprise when in the year 1984 it was reported that two similarly charged plates attract each other set in contact with calcium cholaride [19].

## 1.1 History of Electrostatic Attraction between Similarly Charged Objects

Electrostatic attraction between similarly charged objects is a recently observed phenomenom and was not measured before 1986 by Johan Marra in experiments between two phosphatidylglycerols embedded into an aqueous solution containing calciumchloride, $CaCl_2$ [43], and later by Kjellander et al. [27] between two charged mica surfaces again in the presence of $CaCl_2$.

In simulations this was observed already in 1984 by Gulbrand et al. [19] for two planar surfaces. Much later it was observed by Grosberg-Jensen for two cylindrical rods [17] and by Nordenskiold et al. between many cylindrical rods [41].

These observations led to a huge activity in the field of theoretical physics, especially paving way to the development of field theories to calculate higher order corrections around the Poisson-Boltzmann equation (PB), which had been traditionally used to calculate ion distributions. In the PB-approach, it is assumed that each ion interacts with a mean-field potential created by all the other ions. At the same time, it was already discovered how to calculate the statistics of ions interacting through Coulombic interaction, i.e. the Coulomb gas. Lenard and Edwards were the first ones to show how the grand-canonical partition function could be cast into a field-theoretic form, involving the integration over a field-variable called the fluctuating electrostatic potential [13].

Almost thirty years after this, Podgornik and Zeks [57] were the first ones to show that the saddle-point of the field-theoretic formulation corresponds to the so-called Poisson-Boltzmann (PB) equation, which describes the Poisson law with the Boltzmann distribution for the counter- and coions. Later, Podgornik developed a path-integral technique such that it was possible to calculate loop-corrections around the saddle-point potential, for the system of a one-dimensional Coulombic gas between two planar surfaces [55]. These corrections predict the onset of attraction between two planes, but the problem is that the fluctuation part of the free energy dominates over the PB result in the regime of attraction. This means that although qualitatively correct, the fluctuations around the PB equation do not quantitatively explain either experimental or simulation data.

Finally, in 2000 Roland Netz [51] was able to show that the field theory for a counterion only fluid interacting with a charged surface can be cast into a dimensionless form, where only a single parameter enters the problem: the so-called Strong Coupling (SC) parameter, corresponding to the strength of the electrostatic interaction between counterions and the charged surface. Later, he showed explicitly that in the limit where this coupling parameter goes to zero, one recovers the PB theory, whereas in the opposite limit of an infinitely large coupling parameter there is a novel theoretical regime to be called the SC theory. The biggest difference between the PB and the SC theories is that the SC theory describes the interaction between a single particle and the macrocharge, whereas PB de-

scribes a single particle being in the average potential created by all the other ions and the macrocharge.

Netz also calculated explicitly the electrostatic pressure between two infinite charged walls, and showed that for a certain range of separations between the walls, the pressure is negative, corresponding to a *an attraction between the similarly charged walls*. Later, Naji et al. [50] showed that in the SC limit also two charged rods attract each other if the linear charge density exceeds a certain threshold value.

In this Thesis, our purpose is to extend the SC-theory by Netz, which accounts for effects due to counterions. We do this by introducing also electrolyte salt into the field-theoretic grand-canonical partition function. This is done by adding a Debye-Hückel screening factor into the field-theoretic propagator and subtracting it perturbatively using the virial expansion. Implicitly, this means that the electrolyte salt is weakly coupled to the charged surface, but the counterions are strongly coupled. In addition this also means that our theory describes a system which has a moderate or large amount of added salt. Thus we name the theory the Strong Coupling with Debye-Hückel theory (SC-DH).

## 1.2 Overview of Charged Biopolymers

A polymer is a large molecule, or macromolecule, comprised of repeating structural units called monomers typically connected by chemical bonds. Well-known examples of polymers include plastics and proteins. A very simple example of a polymer is polypropylene, whose repeating units are propane molecules $C_3H_8$, which are bonded to each other via covalent bonds between the carbon atoms.

Biopolymers, instead, are a class of polymers produced by living orgsnisms. Starch, proteins and peptides, DNA and RNA are examples of biopolymers, in which the monomeric units are sugars, amino acids, and nucleotides, respectively.

The major difference between polymers and biopolymers can be found in their structures. Biopolymers often have a well defined structure that typically consists of a hierarchy of different substructures at various length scales. The exact chemical composition of the repetitive units along a biomolecule is called the primary structure. The secondary and/or tertiary structure determines the biological functions of biopolymers, which depend in a complicated way on the primary structure. To the contrary, synthetic polymers have usually much simpler and more random or stochastic structures.

In this Thesis, we consider perhaps the most famous of all biopolymers, deoxyribonucleic acid, more familiarly known as DNA. DNA is a nucleic acid that contains the genetic instructions used in the development and functioning of all known living organisms and some viruses. The main role of DNA molecules is the long-term storage of information. DNA is often compared to a recipe, or a code, since it contains the instructions needed to construct other components of cells, such as proteins. The DNA segments that carry this genetic information are called genes, and other DNA sequences have structural purposes, or are involved in regulating the use of this genetic information.

Physicochemically, DNA consists of two long polymers of units called nucleotides, with backbones made of sugars and phosphate groups joined by ester bonds. Thus we call this "normal" form of DNA a double stranded (ds) ds-DNA. Here the two single strands (ss) run in opposite directions to each other and are therefore anti-parallel. Attached to each sugar in the strand is one of four types of molecules called bases. The two strands are attached to each other through hydrogen bonds between bases on opposite strands. It is usually argued [6] that DNA adopts the double helical conformation mainly due to the hydrophobicity of the bases. The bases want to stay away from water, and in equilibrium at a distance of $3.3$Å away from each other. To the contrary, the phosphates are separated by a distance of $6$Å along the nucleotide. The only conformation to obey both constraints is the double-helix.

DNA looks very different when considered at different length scales. DNA is usually

called a stiff polymer, since the persistence length below which the monomers can be thought to be correlated is very large, being around $50$ nm for B-DNA. However, at somewhat larger scales the secondary structure of DNA shows up, and the molecule starts to bend to form what is called a Gaussian chain in polymer physics, composing of loose strands of larger units, having length equal to one persistence length. The persistence length strongly depends on the electrostatic interaction between the phosphate groups, and this repulsive interaction is responsible for the very stiff primary structure of DNA. However, at length scales way above the persistence length, one can think that the Coulombic interaction is screened out, and the different parts of the chain become uncorrelated. The screening is mainly caused by the physiological concentration of electrolyte salt that is inside the cell. Thus, the secondary structure results mainly from the competition between the elastic bending energy of the DNA backbone and the chemical bonding between these larger units of DNA.

In this Thesis, we consider DNA in both above mentioned length scales. In Sec. 3 we focus on finding the force-extension relation for DNA that is stretched from one end. We use the elasticity theory of Podgornik et al. [56] and combine it with an ad hoc model for base pair bonding proposed by Ahsan et al. [1]. Later we fit the experimental data by Wenner et al. [70] to our theoretical force-extension relation to find the salt-dependence of different parameters. Based on this we suggest that our hybrid model describes the salt dependence of the overstretching force, and also the equation of state of DNA at least for two orders of magnitude of the external force. Later, in Sec. 4, we study the sedimentation of a long DNA chain, exceeding the persistence length by a factor of $100$, and suggest how the sedimentation velocity, diffusion coefficient and the shape of DNA depend on its length. In both applications, the electrolyte salt plays a significant role, and the main purpose of this Thesis is to develop a theoretical framework to model the effect of salt on the physical properties of the DNA chain under consideration.

# 2 Electrostatics of Counterions and Coions around Planar Charged Wall

Electrostatic interactions play a key role in controlling the structure and phase behavior of macroions in aqueous solutions. Examples of biologically relevant macroions are charged biomembranes, stiff polyelectrolytes such as DNA and RNA, or charged colloidal particles. Water solubility of these macroions arises as a consequence of translational entropy of weakly bound counter-ions. Instead of sitting exactly on the charged surface, the counterions want to escape some distance away from the charged ion. In order to understand the behavior of systems composed of charged molecules, one has to understand the counterion and coion distributions associated with each of these charged objects.

The traditional approach towards charged systems has been the Poisson-Boltzmann (PB) approximation, in which the Coulombic interaction between the ions is handled on the mean-field or saddle-point level [40]. This approximation becomes valid in the weak-coupling limit that corresponds to a low surface charge density, low valence of counterions, or high temperature. The common feature for all of these physical factors is that they make the counterion translational entropy to increase, making counterions willing to escape from the charged objects. In the PB theory one can take advantage of the long-range nature of the Coulombic potential, because one charged particle or ion interacts with many surrounding particles at the same time, and the mean-field approach works pretty well and even gives results that are in agreement with experimental and simulation results [40, 51]. However, in many situations the PB approximation breaks down; this happens in the case of multivalent counterions, low temperatures, and for highly charged surfaces. There has been a number of attempts to calculate corrections to the PB theory; correlated density fluctuations around the mean-field distribution, and additional non-electrostatic interactions due to the finite size of the particles [5, 28, 52, 57].

These corrections become especially important for the interaction between similarly charged macroscopic objects. It has been known for more than twenty years from experiments that highly charged planar walls attract each other in the presence of multivalent counterions. This electrostatic attraction may have many practical consequences; for example the restriction of the swelling of calcium clay particles [28], reduced water uptake of charged lamellar membrane systems [71], it has also been observed with surface force apparatus [26], and recently between DNA molecules by using simulation methods [11]. This phenomenon has been tried to explain with different kind of approximate theories described above, but with a consequence that they are valid only for asymptotic distances from the walls.

An alternative approach was discovered by Rouzina and Bloomfield, Shklovskii and coworkers, and later by Moreira and Netz [48, 49, 51, 62]. This led to a development of a new theory, called the Strong Coupling (SC) theory, which becomes exact in the limit of high surface charge, multivalent counterions, or low temperature. Clearly this is the opposite to the PB limit, and thus these two theories asymptotically embrace all possible scenarios, at least for temperatures well above zero, which is biologically relevant. SC is based on the idea that counterions at strongly charged surfaces form an effective two-dimensional layer. Thus we can loosely talk about counterion condensation in the SC theory [42]. Mathematically, the SC theory is a standard virial expansion in terms of the Mayer functions and single particle densities. The SC theory is essentially a one particle theory, since it assumes that the *interaction between ions and the macroion* dominates completely over the ion-ion interactions, thus giving the largest contribution to the partition function and ion densities. In the SC theory attraction between similarly charged objects arises naturally and self-consistently with well-controlled limits to predict the range of validity of the theory.

In addition to counterions, in a biological environment one also encounters other ion types involved in the equilibration process, namely reservoir salt ions. If the reservoir salt concentrations are small compared to real counterion concentration close to charged objects,

one may think that the zero-salt (PB or SC) theories may apply well [40, 51]. However, in biological conditions inside the cell this reservoir salt concentration is typically of the order $[Na^+] = 100$ mM, which corresponds to a relatively small separation between the nearest salt ions. When the salt ion concentration starts to be of the same order as the counterion concentration around the charged object, one may expect to find different equilibrium behavior for the system [62]. Mathematically, this corresponds to a fact that the Coulombic interaction is screened out and we are led back to the PB or Debye-Hückel (DH) regimes.

In the existing literature, there is no consistent formulation for the partition function of counterions around a macroscopic charged object in the SC limit with bulk salt included. Thus, we want to extend the electrostatics formalism to consistently take into account bulk salt effects. The main results are presented in a general form in Sec. 2.1, where we present the leading order results derived in Article I of this Thesis, and the next-leading corrections to the ion densities considered in Article II. It turns out that especially the first order densities contain very rich physics that shows up in the number of different length scales pertinent to the theory.

Before we formulate the theoretical model in a general form, we want to introduce the relevant length scales and parameters in the problem, and show by scaling arguments what should be expected from the mathematical formalism. The most important length scale in the problem of counterions and charged macroscopic object is the *Gouy-Chapman* (GC) length, defined as

$$\mu = 1/2\pi q_c \sigma_s l_B \propto q_c T/\sigma, \tag{2.1}$$

where $q_c$ is the counterion valence, $\sigma_s$ is the surface charge density and $l_B = e^2/4\pi\epsilon k_B T$ is the Bjerrum length, which measures the distance at which two unit charges interact with thermal energy; in water $l_B \simeq 0.71$ nm at room temperature. Here $e$ is the unit charge, $\epsilon$ is the dielectric constant, $T$ is temperature, and $k_B$ is the Boltzmann factor. The GC length measures the distance from the charged surface at which the electrostatic potential energy of an ion interacting with the surface reaches the thermal energy $k_B T$. In terms of

physics, this length scale measures the average distance of ions from the charged object.

Later, in defining the whole field-theoretic formulation for the problem, it turns out that we can expand the partition function around the dimensionless parameter that is defined in terms of the the GC length and the Bjerrum length as

$$\Xi = 2\pi q_c^3 l_B^2 \sigma_s \propto q_c^3 \sigma / T^2, \tag{2.2}$$

which we call the Strong Coupling parameter, in the spirit of the SC theory á la Netz [51].

A third very important length scale, which can be related to the two previous ones, is the lateral distance between the charges on the charged object, which corresponds to the surface charge density of the object. It is defined by thinking that due to electroneutrality one ion on average occupies a circle of radius $a_\perp$ as

$$\pi a_\perp^2 = q_c / \sigma_s, \tag{2.3}$$

which leads to

$$a_\perp = \sqrt{(q_c / \pi \sigma_s)} = \sqrt{2\Xi}\mu, \tag{2.4}$$

and is independent of temperature, thus allowing to approach the zero temperature limit [67]. This lateral distance is important, because in the SC regime we can express the concentration of the two-dimensional counterion layer as [62]

$$n_s = \frac{\sigma_s}{q_c \mu} = \frac{1}{\pi a_\perp^2 \mu}. \tag{2.5}$$

The concentration of this type of strongly correlated diffuse counterion layer should be independent of the bulk ion concentration, as long as the ionic strength

$$I = \frac{1}{2} \sum_i \Lambda_i q_i^2, \tag{2.6}$$

is significantly less than $n_s$, i.e. $I \ll n_s$. Here $\Lambda_i$ and $q_i$ are the concentrations and valences of different ion types. This clearly means that counterion concentration on the surface should be much larger than the reservoir salt concentration.

Furthermore, we introduce a very important length-scale describing the range of the electrostatic interaction, namely the *Debye screening length* defined as

$$l_{DH}^{-2} \equiv \kappa^2 = 8\pi l_B I. \tag{2.7}$$

It has a clear physical meaning, since it measures the distance at which the Coulomb interaction becomes screened by the surrounding ions. Now we can easily see the connection between the Debye length and the criterion $I \ll n_s$, since this can be written as

$$\kappa\mu \ll 1. \tag{2.8}$$

It was shown in Article I of the Thesis that the parameter $\kappa\mu$ together with $\Xi$ completely determines the zeroth order ion densities.

In Article II we extend our goal to calculate also the first order ion densities that explicitly take into account the ion-ion interactions through the Mayer functions. This means that oppositely charged particles attract each other, and want to stick to as close to each other as possible. Formally, we end up with infinite interaction terms, unless we set a hardcore interaction potential between all the particles. There are many ways of doing that such as using Lennard-Jones forces etc., but here we follow the simplest route by handling the short range forces by delta-functions. This means that all the interaction integrals are restricted from below by a hardcore radius $a$ that should correspond to the experimentally measured value of the ion radius of the ion type under consideration. Thus, we get an extra parameter, which enters as a combination of ion diameter $2a$, valences of oppositely charged ions, here $q_-$ and $q_c$ (being typically larger than $q_+$) and the Bjerrum length, and due to Mayer function expansion always enters as an exponential of the combination

$$\frac{q_c q_- l_B}{2a}. \tag{2.9}$$

Its contribution to ion-densities becomes the more important the smaller the numerical value of ion radius is, implying ion pairing into the so-called Bjerrum pairs.

Later, in Sec. 2.1 we present the results of the derivations done in Articles I and II. We evaluate the ion densities around an arbitrary macroscopic charged object interacting

with its counterions and with an arbitrary concentration of bulk salt that is electroneutral by itself. We calculate the ion densities in the theoretically cumbersome regime $\Xi \gg 1, \kappa\mu \geq 0$ in the phase diagram of the system. This regime also contains the phase line $\kappa\mu = \Xi^{1/2}$, corresponding to the transition from the strong coupling regime to the weak coupling, or DH-regime. We call the novel regime in the phase diagram between the zero-salt SC and DH a *Strong Coupling with Weak Debye-Hückel* (SC-DH) regime, which corresponds to $\Xi \gg 1$ and $2a/q_c^2 l_B \ll \kappa\mu \ll \Xi^{1/2}$. Mathematically, this formulation corresponds to a standard virial approximation, meaning that all ion concentrations are small. From this regime one can interpolate to the limit $\kappa\mu \to \infty$ by re-expanding the Mayer functions in terms of the Debye-Hückel potential. This is shown for the case of one infinite plate in Sec. 2.1.2. However, we will also show that in the zero salt limit all the higher order densites contain terms being equally large in magnitude as the zeroth order density. This means that the novel SC-DH theory works only in the presence of a moderate or large concentration of excess salt.

Later in Sec. 2.1, we explicitly obtain results for the case of a macroscopic charged body being one infinite wall. We calculate the ion densities to zeroth order and to first order in ion fugacities $\Lambda_\alpha$. This way we obtain criteria for the validity of the results also as a function of the distance from the walls, and see that it is not self-evident to talk about different parameter regimes per se, but that one also sees different kind of physics for different distances from the wall.

Finally, Sec. 2.2 summarizes all the key points studied in Articles I and II. In the very end, we discuss possible applications of our formalism to study the interaction between DNA type of biopolymers.

## 2.1 Field Theory for Co- and Counterions Around Infinite Charged Wall

We start by constructing the partition function for a system of $N_C$ positively charged counterions of valence $q_C$ in a vicinity of a continuous charged macroscopic object of surface charge distribution $-\sigma(\mathbf{r})$. These are surrounded by an external salt bath, which is composed of $N_+$ positively charged ions of valence $q_+$ and $N_-$ negatively charged ions of valence $q_-$, both interacting with the macroscopic body and its counterions. The idea in this derivation is that $N_C$ counterions exactly neutralize the macroscopic charge, whereas the remaining $N_+$ positive ions and $N_-$ negative ions form an electroneutral screening medium such that $q_+N_+ = q_-N_-$. All the ions and the macroscopic charged object interact via the Coulomb potential $v_c(\mathrm{r}) = l_B/|\mathbf{r}|$. The grand-canonical partition function $\mathcal{Q}$ for this system can be cast into a field-theoretic form, as was shown in Articles I and II of this Thesis, and it can be written with the help of the field variable $\phi$, corresponding to a fluctuating electrostatic field as

$$\mathcal{Q} \equiv \int \frac{\mathcal{D}\phi}{\mathcal{Z}_{DH}} e^{-\tilde{H}[\phi]}, \tag{2.10}$$

where the Hamiltonian is

$$\begin{aligned}\mathcal{H}[\phi] = \frac{1}{2}\int \mathrm{d}\mathbf{r}\mathrm{d}\mathbf{r}'\phi(\mathbf{r})v_{DH}^{-1}(\mathbf{r}-\mathbf{r}')\phi(\mathbf{r}') - i\frac{q_c}{2\pi}\int \mathrm{d}\mathbf{r}\phi(\mathbf{r})\sigma(\mathbf{r}) - \frac{\Lambda_c}{2\pi}\int \mathrm{d}\mathbf{r} e^{-iq_c\phi(\mathbf{r})+\frac{1}{2}q_c^2 v_{DH}(\mathbf{0})} \\ - \frac{\Lambda_+}{2\pi}\int \mathrm{d}\mathbf{r}\left[e^{-iq_+\phi(\mathbf{r})+\frac{1}{2}v_{DH}(\mathbf{0})} + \frac{1}{2}q_+^2\phi(\mathbf{r})^2 - \frac{1}{2}q_+^2 v_{DH}(\mathbf{0})\right] \\ - \frac{\Lambda_-}{2\pi}\int \mathrm{d}\mathbf{r}\left[e^{+iq_-\phi(\mathbf{r})+\frac{1}{2}v_{DH}(\mathbf{0})} + \frac{1}{2}q_-^2\phi(\mathbf{r})^2 - \frac{1}{2}q_-^2 v_{DH}(\mathbf{0})\right],\end{aligned} \tag{2.11}$$

and the DH propagator is given by

$$v_{DH}^{-1}(\mathbf{r}-\mathbf{r}') = \frac{1}{4\pi l_B}[-\nabla^2 + \kappa^2]\delta(\mathbf{r}-\mathbf{r}'), \tag{2.12}$$

having a well-known free space inverse of

$$v_{DH}(\mathbf{r}) = \frac{l_B}{|\mathbf{r}|}e^{-\kappa|\mathbf{r}|}. \tag{2.13}$$

Here, we explicitly add the screening into the Coulombic propagator, and later subtract it perturbatively by using the virial expansion. This works as long as the $\phi^2$ terms in the exponential are small compared to unity, allowing the expansion of the exponential of $\phi^2$. Later, after carrying out the virial expansion in terms of all ion densities, one cannot force $\kappa \to 0$ anymore. Otherwise, it would happen that the expanded $\phi^2$-terms would become more and more important to the higher orders in ion densities. Thus, we expect that the virial expansion introduced here works properly only in the limit of a large concentration of excess salt.

The main result of Article II are the grand-canonical densities of all ion types in the SC limit $\Xi \to \infty$, corresponding to the virial expansion with respect to all ion-species. For the counterions one obtains the following density [61]

$$\begin{aligned}
\rho_c(\mathbf{r}_1) &= \Lambda_c^0 e^{u(\mathbf{r}_1)} + \big\{\Lambda_c^1 e^{u(\mathbf{r}_1)} \\
&\quad -(\Lambda_c^0)^2 \int \mathrm{d}\mathbf{r}_2 e^{-q_c u(\mathbf{r}_1)-q_c u(\mathbf{r}_2)} \left[1 - e^{-q_c^2 v_{DH}(\mathbf{r}_1-\mathbf{r}_2)}\right] \\
&\quad -\Lambda_c^0\Lambda_-^0 \int \mathrm{d}\mathbf{r}_2 e^{-q_c u(\mathbf{r}_1)+q_- u(\mathbf{r}_2)} \left[1 - e^{+q_c q_- v_{DH}(\mathbf{r}_1-\mathbf{r}_2)}\right] \\
&\quad -\Lambda_c^0\Lambda_+^0 \int \mathrm{d}\mathbf{r}_2 e^{-q_c u(\mathbf{r}_1)-q_+ u(\mathbf{r}_2)} \left[1 - e^{-q_c q_+ v_{DH}(\mathbf{r}_1-\mathbf{r}_2)}\right] \\
&\quad -\frac{\kappa^2}{8\pi l_B}\Lambda_c^0 \int \mathrm{d}\mathbf{r}_2 e^{\mp q_\pm u(\mathbf{r}_1)} [+q_c v_{DH}(\mathbf{r}_1-\mathbf{r}_2) - u(\mathbf{r}_2)]^2 \Big\} + \mathcal{O}\left(\Lambda_\alpha^3\right) \\
&\equiv \rho_c^0(\mathbf{r}_1) + \rho_c^1(\mathbf{r}_1) + \mathcal{O}\left(\rho_\alpha^2\right),
\end{aligned} \tag{2.14}$$

and for the negative and positive salt ions we find

$$\begin{aligned}
\rho_\pm(\mathbf{r}_1) &= \Lambda_\pm^0 e^{\mp q_\pm u(\mathbf{r}_1)} + \big\{\Lambda_\pm^1 e^{\mp q_\pm u(\mathbf{r}_1)} \\
&\quad -(\Lambda_\pm^0)^2 \int \mathrm{d}\mathbf{r}_2 e^{\mp q_\pm u(\mathbf{r}_1)\pm q_\mp u(\mathbf{r}_2)} \left[1 - e^{-q_\pm^2 v_{DH}(\mathbf{r}_1-\mathbf{r}_2)}\right] \\
&\quad +\frac{1}{2} q_\pm^2 [\pm q_\pm v_{DH}(\mathbf{r}_1-\mathbf{r}_2) - u(\mathbf{r}_2)]^2 \\
&\quad -\Lambda_\pm^0\Lambda_c^0 \int \mathrm{d}\mathbf{r}_2 e^{\mp q_\pm u(\mathbf{r}_1)-q_c u(\mathbf{r}_2)} \left[1 - e^{\mp q_c q_\pm v_{DH}(\mathbf{r}_1-\mathbf{r}_2)}\right] \\
&\quad -\Lambda_\pm^0\Lambda_\mp^0 \int \mathrm{d}\mathbf{r}_2 e^{\mp q_\pm u(\mathbf{r}_1)\pm q_\mp u(\mathbf{r}_2)} \left[1 - e^{+q_\pm q_\mp v_{DH}(\mathbf{r}_1-\mathbf{r}_2)}\right] \\
&\quad -\frac{\kappa^2}{8\pi l_B}\Lambda_\pm \int \mathrm{d}\mathbf{r}_1 e^{\mp q_\pm u(\mathbf{r}_1)} [\pm q_\pm v_{DH}(\mathbf{r}_1-\mathbf{r}_2) - u(\mathbf{r}_2)]^2 \Big\} + \mathcal{O}\left(\Lambda_\alpha^3\right) \\
&\equiv \rho_c^0(\mathbf{r}_1) + \rho_c^1(\mathbf{r}_2) + \mathcal{O}\left(\rho_\alpha^2\right).
\end{aligned} \tag{2.15}$$

Here the single particle interaction energy with the charged surface plays a dominant role in determining the ion densities, and is given by

$$u(\mathbf{r}) = \frac{1}{2\pi}\int \mathrm{d}\mathbf{r}'\sigma(\mathbf{r}')[v_{DH}(\mathbf{r}') - v_{DH}(\mathbf{r}-\mathbf{r}')], \tag{2.16}$$

where $\Lambda_\alpha$ and $q_\alpha$ stand for the fugacities and valences of all ion types.

The ion fugacities $\Lambda_\alpha$ are determined in the grand canonical ensemble by requiring that the integral of the total charge density over the domain of ions equals the total charge of the surface of the macroion. The normalization is made order by order in ion densities as

$$\begin{aligned}\int \mathrm{d}\mathbf{r}\left(q_c\rho_c^0(\mathbf{r}) + q_+\rho_+^0(\mathbf{r}) - q_-\rho_-^0(\mathbf{r})\right) &= \int \mathrm{d}\mathbf{r}\sigma(\mathbf{r});\\ \int \mathrm{d}\mathbf{r}(q_c\rho_c^k(\mathbf{r}) + q_+\rho_+^k(\mathbf{r}) - q_-\rho_-^k(\mathbf{r})) &= 0,\end{aligned} \tag{2.17}$$

where each one of the equations actually contains two parts, namely an infinite bulk part and a finite normalizable part. This is a consequence of the fact that in the presence of screening, none of the ion-densities drop to zero infinitely far away from the charged macroion, but instead approach a finite bulk concentration. In other words, all the ions have a finite probability of getting into the bulk. This means that we have now three unknown variables $\{\Lambda_c^k, \Lambda_+^k, \Lambda_-^k\}$ to all orders in densities, such that on top of Eqs. (2.17), one also has to expand Eqs. (2.6) and (2.7) to all orders as

$$\begin{aligned}8\pi l_B(q_+^2\Lambda_+^0 + q_-^2\Lambda_-^0) &= \kappa^2,\\ q_+^2\Lambda_+^k + q_-^2\Lambda_-^k &= 0, \qquad k>1.\end{aligned} \tag{2.18}$$

Eqs. (2.17) and (2.18) uniquely determine the fugacities of all ion types to any order, and we will use them in what follows for an infinite charged plate.

### 2.1.1 Zeroth Order Densities

Let us consider the zeroth order ion densities for the case of a charged plane, located at $z = 0$, which is impenetrable for the counterions and thus restricts all mobile ions to the

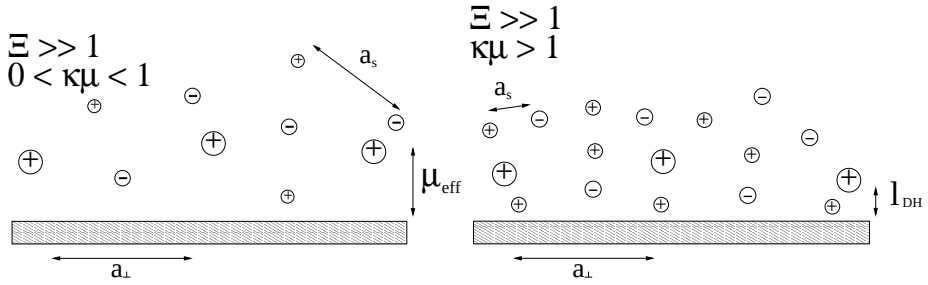


(a) $\kappa\mu \ll 1$ (b) $\kappa\mu \geq 1$

**Figure 2.1**: An infinite charged plate interacting with ions: (a) For bulk salt concetration much smaller than $n_s$, the distance between the salt ions $a_s = n_s^{-1/3}$ is much larger than the Gouy-Chapman length. In this regime we can consider salt as a small perturbation around the pure SC results [51]. b) When salt ion concentration starts to be of the same magnitude as counterion concentration, the salt ions penetrate between counterions and charged surface, validating the Debye screening picture [60].

positive half space $z > 0$. The charge distribution is given by the Dirac delta function $\sigma(\mathbf{r}) = \sigma_s\delta(z)$, where $\sigma_s$ is the two-dimensional surface charge density. The rescaled single-particle interaction energy created by one charged wall, defined in Eq. (2.16), is given by

$$u(z) = \frac{1}{q_c\kappa\mu}[1 - e^{-\kappa z}], \tag{2.19}$$

and reduces correctly to $\kappa \to 0$ studied in [51] .

The zeroth order counterion density can be calculated from Eq. (2.14) and Eq. (2.17) as

$$\rho_c^0(z) = \Lambda_c^0 e^{-[1-e^{-\kappa z}]/\kappa\mu}; \tag{2.20}$$

and for salt ions

$$\rho_\pm^0(z) = \Lambda_\pm^0 e^{\mp q_\pm[1-e^{-\kappa z}]/q_c\kappa\mu}. \tag{2.21}$$

The normalization condition for the ion distributions reads as

$$\int \mathrm{d}z[\rho_c^0(z) + \rho_+^0(z) - \rho_-^0(z)] = \int \mathrm{d}z\sigma(z) = \sigma_s. \tag{2.22}$$

Next we expand the fugacities according to

$$\Lambda_\alpha = \Lambda_\alpha^0 + \Lambda_\alpha^1 + \mathcal{O}(\Lambda_\alpha^2), \tag{2.23}$$

and insert this to the normalization condition Eq. (2.22). Here we also rescale all the fugacities by $q_c\sigma_s/\mu$, such that they become dimensionless. After a little bit of algebra we find the rescaled counterion fugacity

$$\begin{aligned}\frac{q_c\Lambda_c^0}{\sigma_s/\mu} &= \kappa\mu e^{1/\kappa\mu}\left\{2[q_+e^{(q_++q_-)/(q_c\kappa\mu)}+q_-]-q_c\kappa\mu e^{q_-/(q_c\kappa\mu)}(f[q_+/(q_c\kappa\mu)]-f[-q_-/(q_c\kappa\mu)])\right\}: \\ &\left\{2f[1/(\kappa\mu)](q_-+q_+e^{(q_++q_-)/(q_c\kappa\mu)})+f[q_+/(q_c\kappa\mu)]-f[-q_-/(q_c\kappa\mu)]\right\} \\ &\xrightarrow{\kappa\mu\to 0} 1-\kappa\mu-(\frac{1}{2}\frac{q_c^2}{q_+^2}-1)(\kappa\mu)^2.\end{aligned} \tag{2.24}$$

The salt ion fugacities expressed with the help of this are

$$\begin{aligned}\frac{q_c\Lambda_+^0}{\sigma_s/\mu} =&[0.5q_c(\kappa\mu)^2-q_-e^{-(q_++q_-)/(q_c\kappa\mu)}\Lambda_c^0]: \\ &[q_++q_-e^{-(q_++q_-)/(q_c\kappa\mu)}] \\ &\xrightarrow{\kappa\mu\to 0}\frac{1}{2}\frac{q_c^2}{q_+^2}(\kappa\mu)^2;\end{aligned} \tag{2.25}$$

$$\begin{aligned}\frac{q_c\Lambda_-^0}{\sigma_s/\mu} &= e^{-q_-/(q_c\kappa\mu)}[e^{-q_+/(q_c\kappa\mu)}\Lambda_+^0+e^{-1/(\kappa\mu)}\Lambda_c^0] \\ &\xrightarrow{\kappa\mu\to 0}\frac{q_+}{q_-}\frac{1}{2}\frac{q_c^2}{q_+^2}(\kappa\mu)^2e^{-(q_++q_-)/(q_c\kappa\mu)},\end{aligned} \tag{2.26}$$

where we have defined an auxiliary function

$$f[x] = \mathrm{E}i[x]-\gamma-\log[|x|]. \tag{2.27}$$

Here we have used the standard "Mathematica" names for special functions, and $\gamma$ is the Euler gamma given by $\gamma = 0.57....$ The final limiting form arises in the limit $\kappa\mu \to 0$, which we are especially interested in. This leads to the final expression for the zeroth order density as

$$\begin{aligned}\rho_c^0(z) &= \frac{\kappa\mu}{\mathrm{E}i[1/\kappa\mu]-\gamma+\log(\kappa\mu)}\exp-(1-e^{-\kappa z})/\kappa\mu \\ &\xrightarrow{\kappa\mu\to 0} e^{-z/\mu}[1-\kappa\mu(1-\frac{1}{2}[\frac{z}{\mu}]^2)].\end{aligned} \tag{2.28}$$

First of all, this demonstrates that against our expectations, the zeroth order density of our theory agrees exactly with the zero salt SC theory á la Netz, and is given by

$$\rho_c^0(z) \xrightarrow{\kappa\mu\to 0} e^{-z/\mu}. \tag{2.29}$$

Furthermore, Eq. (2.28) indicates that the density is reduced close to the wall compared to the zero salt case of Netz. This means that counterions are more spread out to the surrounding space in the presence of salt.

However, as was already mentioned at the beginning of Sec. 2.1, in this artificial zero-salt limit all the higher orders will contain terms that are increasingly important, thus invalidating the virial expansion. We will show in Sec. 2.1.2 that this comes out already to first order in ion densities.

The next-leading corrections to ion densities can in principle be evaluated from Eqs. (2.14) and (2.15). The final expressions are so complicated that we have to resort to further approximations in order to get an analytical solution.

### 2.1.2 First Order Densities

First order densities cannot be evaluated in a closed form and thus one needs to resort to further approximations. Before introducing these, let's calculate exactly the interaction integral between the DH salt and the ion densities, i.e.

$$\begin{aligned} I_{DH}(q_\alpha, z) &= \int \mathrm{d}\mathbf{r}'[\pm q_\alpha v_{DH}(\mathbf{r}-\mathbf{r}') - u(\mathbf{r}_2)]^2 \\ &= 2\pi\frac{q_\alpha^2 l_B^2}{2\kappa}(e^{-2\kappa z} - 2\kappa z_1 \Gamma[0, 2\kappa z]) \\ &\mp 2\pi\frac{q_\alpha l_B}{q_c\kappa^2\mu}(ze^{-\kappa z} - e^{-\kappa z}/2\kappa) \\ &\xrightarrow{\kappa\mu\to 0} 2\pi\left[\frac{q_\alpha^2 l_B^2}{2\kappa} \mp \frac{q_\alpha l_B}{q_c\kappa^2\mu}[\frac{3}{2}z - \frac{1}{2\kappa}]\right], \end{aligned} \tag{2.30}$$

where $\Gamma[0, x]$ is the incomplete gamma function of zeroth order. This has a smooth limit to the zero salt case if we renormalize the last term of $I_{DH}(q_\alpha, z)$ by subtracting its value at $z = 0$ from it. This can be done by including these constant terms into first order fugacities, to be determined later from Eqs. (2.17) and (2.18). Thus, we can write the

interaction integral between the DH salt and ion densities as

$$\begin{aligned} I_{DH}(q_\alpha, z) &= \int \mathrm{d}\mathbf{r}'[\pm q_\alpha v_{DH}(\mathbf{r}-\mathbf{r}') - u(\mathbf{r}_2)] \\ &= 2\pi \frac{q_\alpha^2 l_B^2}{2\kappa}(e^{-2\kappa z} - 2\kappa z \Gamma[0, 2\kappa z]) \\ &\mp 2\pi \frac{q_\alpha l_B}{q_c \kappa^2 \mu}(z e^{-\kappa z} + (1-e^{-\kappa z})/2\kappa). \end{aligned} \tag{2.31}$$

After this, one can easily solve the bulk part of the normalization integral Eq. (2.17) by noticing that the Mayer functions $1 - e^{-q_\alpha q_\beta v_{DH}(\mathbf{r})}$ vanish exponentially fast at $|\mathbf{r}_2| \to \infty$ and do not have any contribution to bulk values. Thus, the first-order bulk neutrality reads as

$$\begin{aligned} &q_c \rho_c^0(\infty)[\Lambda_c^1/\Lambda_c^0 + \frac{1}{8\kappa\mu}] + q_+ \rho_+^0(\infty)[\Lambda_+^1/\Lambda_+^0 + \frac{q_+}{8 q_c \kappa\mu}] \\ &= q_- \rho_-^0(\infty)[\Lambda_-^1/\Lambda_-^0 - \frac{q_-}{8 q_c \kappa\mu}]. \end{aligned} \tag{2.32}$$

This combined with Eq. (2.17) gives a finite solution for $\{\Lambda_c, \Lambda_+, \Lambda_-\}$ for all values of $\kappa\mu$.

In what follows, we present three cases where the ion-ion interaction term described by the Mayer functions can be calculated approximately. First one of them is the artificial limit $\kappa\mu \to 0$, which we do not expect to give the right zero salt SC limit [51]. The second one of them is the regime where our theory becomes valid, and the third one is the excess salt limit where all the interactions are screened completely.

### (i) Artificial zero salt limit

In the extremely small salt concentration limit, one can use the following strategy. We assume that the Debye screening length $\kappa^{-1}$ is the largest length scale, and evaluate the integrals over the Mayer function in Eqs. (2.14) and (2.15) only up to $\kappa^{-1}$. This allows one to expand the single-particle interaction as

$$u(z) \xrightarrow{\kappa\mu \to 0} \frac{z}{q_c \mu}, \tag{2.33}$$

and the two-particle interaction in the Mayer function can be treated as a Coulombic interaction, i.e. $v_{DH}(\mathbf{r}) \xrightarrow{\kappa\mu\to 0} v_c(\mathbf{r})$. After these approximations the density-density interaction terms in Eqs. (2.14) and (2.15) read as

$$
\begin{aligned}
I_{\alpha,\beta}(z) &\equiv \Lambda_\alpha^0 \int \mathrm{d}\mathbf{r}' e^{\pm q_\alpha u(z')} \left[1 - e^{+q_c q_- v_{DH}(\mathbf{r}-\mathbf{r}')}\right] \\
&\xrightarrow{\kappa\mu\to 0} \Lambda_\alpha^0 \int \mathrm{d}\mathbf{r}' e^{\pm q_\alpha u(z')} \left[1 - e^{+q_c q_- v_c(\mathbf{r}-\mathbf{r}')}\right] \\
&\xrightarrow{\Xi\to\infty} \frac{q_c^2}{q_\alpha^2}\frac{\Lambda_\alpha^0}{\Xi} e^{\mp q_\alpha z/(q_c\mu)} \\
&\times \Big\{ \pm [z^3 e^{\pm\frac{q_\alpha z}{q_c\mu} + q_\alpha q_\beta l_B/z} - (2a)^3 e^{\pm\frac{q_\alpha 2a}{q_c\mu} + q_\alpha q_\beta l_B/2a}]|_{z\geq 2a} \\
&\mp [(\kappa^{-1})^3 e^{\mp\frac{q_\alpha}{q_c\kappa\mu} + q_\alpha q_\beta \kappa l_B} - (2a)^3 e^{\mp\frac{q_\alpha 2a}{q_c\mu} + q_\alpha q_\beta l_B/2a}] \Big\} \\
&+ \Lambda_\alpha^0 e^{\mp q_\alpha z/(q_c\mu)} \left\{ \pm\frac{1}{2}\Lambda_\alpha^0 \left(2 + \frac{q_\alpha z}{q_c\mu}[\mp 2 + q_\alpha z/(q_c\mu)]\right) \right. \\
&\left. \mp e^{\mp(q_\alpha z/(q_c\mu) + \kappa^{-1})/\mu} \left(2 + \frac{q_\alpha}{q_c\kappa\mu}[\pm 2 + q_\alpha/(q_c\kappa\mu)]\right) \right\} \\
&\equiv \frac{q_c^2}{q_\alpha^2}\frac{\Lambda_\alpha^0}{\Xi} e^{\mp q_\alpha z/(q_c\mu)} \left[\pm g_\pm(\pm z, \pm 2a, q_\alpha, q_\beta)\right. \\
&\left. \mp g_\pm(\mp\kappa^{-1}, \mp 2a, q_\alpha, q_\beta) + s_\alpha(z)\right].
\end{aligned}
\tag{2.34}
$$

Here the second limit actually holds only if $q_c\mu$ is smaller than the ion diameter $2a$. Here we have also defined the auxiliary functions

$$
\begin{aligned}
g_\pm(z, 2a, q_\alpha, q_\beta) = z^3 e^{\pm q_\alpha z_1/(q_c\mu) \pm q_\alpha q_\beta l_B/z_1} \\
- (2a)^3 e^{\pm q_\alpha 2a/(q_c\mu) \pm q_\alpha q_\beta l_B/2a},
\end{aligned}
\tag{2.35}
$$

and

$$
\begin{aligned}
s_\alpha(z) = \frac{1}{2}\{\pm(2 + \frac{q_\alpha z_1}{q_c\mu}[\mp 2 + q_\alpha z_1/(q_c\mu)]) \\
\mp e^{\mp(q_\alpha z_1/(q_c\mu) + \kappa^{-1})/\mu}(2 + \frac{q_\alpha}{q_c\kappa\mu}[\pm 2 + q_\alpha/(q_c\kappa\mu)])\}.
\end{aligned}
\tag{2.36}
$$

In Eq. (2.34) the first term describes the density at the *second layer* behind the condensed layer of counterions close to the surface. On the other hand, the second term makes a small contribution to ion densities in the *first layer*, being however smaller than the first term in accord with the SC theory.

Furthermore, the Debye-Hückel salt interaction with ion densities is given by Eq. (2.31), and gives a contribution $\kappa^2/(8\pi l_B) I_{DH}(q_\alpha, z) \to \mp \frac{3 q_\alpha z}{8\mu}$ to ion densities in the $\kappa\mu \to 0$ limit, which is *not small compared to the zeroth order density*, but actually of the same order. Once again, this confirms that SC-DH theory does not give right predictions in the zero salt limit.

With the help of the previous expressions we can evaluate the limiting form of the first order counterion density as

$$\begin{aligned}
&\rho_c^1(z) = \rho_c^0(z) \\
&\times \left\{ \Lambda_c^1/\Lambda_c^0 + 2\pi \Lambda_c^0 \mu^3 e^{-z/\mu} \left[ g_-(+z, 2a, q_c, q_c) - g_-(-\kappa^{-1}, -2a, q_c, q_c) \right] \right. \\
&+ 2\pi \frac{q_c^2}{q_+^2} \Lambda_+^0 \mu^3 e^{-q_+ z/(q_c \mu)} \left[ g_-(+z, 2a, q_+, q_c) - g_-(-\kappa^{-1}, -2a, q_+, q_c) \right] \\
&+ 2\pi \frac{q_c^2}{q_-^2} \Lambda_-^0 \mu^3 e^{+q_- z/(q_c \mu)} \left[ g_+(-z, -2a, q_-, q_c) - g_-(\kappa^{-1}, 2a, q_-, q_c) \right] \\
&\left. + s_c(z) + s_+(z) + s_-(z) - \frac{\kappa^2}{8\pi l_B} I_{DH}(q_c, z) \right\},
\end{aligned} \tag{2.37}$$

where the first-order fugacity is determined later by normalization. Salt ion densities are determined similarly as

$$\begin{aligned}
&\rho_+^1(z) = \rho_+^0(z) \\
&\times \left\{ \Lambda_+^1/\Lambda_+^0 + 2\pi \Lambda_c^0 e^{-z/\mu} \left[ g_-(+z, 2a, q_c, q_+) - g_-(-\kappa^{-1}, -2a, q_c, q_+) \right] \right. \\
&2\pi \frac{q_c^2}{q_+^2} \Lambda_+^0 e^{-q_+ z/(q_c \mu)} \left[ g_-(+z, 2a, q_+, q_+) - g_-(-\kappa^{-1}, -2a, q_+, q_+) \right] \\
&2\pi \frac{q_c^2}{q_-^2} \Lambda_-^0 e^{+q_- z/(q_c \mu)} \left[ g_+(-z, -2a, q_-, q_+) - g_-(\kappa^{-1}, 2a, q_-, q_+) \right] \\
&\left. + s_c(z) + s_+(z) + s_-(z) - \frac{\kappa^2}{8\pi l_B} I_{DH}(q_+, z) \right\},
\end{aligned} \tag{2.38}$$

and

$$\begin{aligned}
&\rho_-^1(z) = \rho_-^0(z) \\
&\times \Big\{ \Lambda_-^1/\Lambda_-^0 + 2\pi\Lambda_c^0 e^{-z/\mu} \left[ g_+(+z, 2a, q_c, q_-) - g_+(-\kappa^{-1}, -2a, q_c, q_-) \right] \\
&2\pi \frac{q_c^2}{q_+^2} \Lambda_+^0 e^{-q_+ z/(q_c\mu)} \left[ g_+(+z, 2a, q_+, q_-) - g_+(-\kappa^{-1}, -2a, q_+, q_-) \right] \\
&2\pi \frac{q_c^2}{q_-^2} \Lambda_-^0 e^{+q_- z/(q_c\mu)} \left[ g_+(-z, -2a, q_-, q_-) - g_-(\kappa^{-1}, 2a, q_-, q_-) \right] \\
&+ s_c(z) + s_+(z) + s_-(z) - \frac{\kappa^2}{8\pi l_B} I_{DH}(q_-, z) \Big\} .
\end{aligned} \tag{2.39}$$

From Eqs. (2.37), (2.38) and (2.39) we can extract the $\kappa\mu \to 0$ result by counting only the smallest powers of $\kappa\mu$. This way all the ion-ion interaction terms become small compared to entropic contributions, and we find for the counterions the zero-salt limit as

$$\begin{aligned}
\rho_c^1(z) \xrightarrow{\kappa\mu\to 0} \rho_c^0(z) \Bigg[ & \frac{\Lambda_c^1}{\Lambda_c^0} + \frac{3z/\mu}{8} + \frac{1}{2\Xi}([\frac{z}{\mu}]^2 - 2\frac{z}{\mu}) \\
& + \frac{q_c^2}{2q_+q_-^3} \frac{\kappa^2}{l_B} [(2a)^3 e^{+q_-(z-2a)/(q_c\kappa\mu) + q_- q_c l_B/(2a)} - z^3 e^{+q_- q_c l_B/z}] \\
& - \frac{q_c^2}{2q_+q_-^3} \frac{1}{\kappa l_B} e^{+\frac{q_-}{q_c\kappa\mu}(1+\kappa z) + q_- q_c \kappa l_B} ] \Bigg] \\
\overset{*}{\to} & \left[ \Lambda_c^1 + \frac{3z/\mu}{8} + \frac{1}{2\Xi}([\frac{z}{\mu}]^2 - 2\frac{z}{\mu}) \right] .
\end{aligned} \tag{2.40}$$

Here one needs to notice that the negative ion interaction with the counterions in the second limit (*) is small only if the exponential of the following expression satisfies

$$q_c q_- \frac{l_B}{z} - \frac{(q_+ + q_-)}{q_c\kappa\mu} \ll 0, \tag{2.41}$$

and because $z \geq 2a$ in the interaction terms, this translates into

$$\frac{2\tilde{a}}{\Xi} > \frac{q_-}{(q_+ + q_-)} \kappa\mu \propto \kappa\mu, \tag{2.42}$$

which was also mentioned in Eq. (19) of Ref. [60]. This means that one cannot talk about the ion radius and salt separately, but they are intimately coupled such that one cannot reduce $a$ to zero without removing all the salt. However, the opposite can be done, i.e., salt can be removed such that we get zero salt in the presence of a finite ion size.

In a similar way we obtain the zero-salt first order positive ion density as

$$\rho_+^1(z) \xrightarrow{\kappa\mu\to 0} \rho_+^0(z)\left[\Lambda_+^1/\Lambda_+^0 + \frac{3q_+ z/\mu}{8q_c} + \frac{1}{2\Xi}([\frac{z}{\mu}]^2 - 2\frac{z}{\mu})\right], \tag{2.43}$$

and for the negative ion density

$$\rho_-^1(z) \xrightarrow{\kappa\mu\to 0} \rho_-^0(z)\left[\Lambda_-^1/\Lambda_-^0 - \frac{3q_+ z/\mu}{8q_c} + \frac{1}{2\Xi}([\frac{z}{\mu}]^2 - 2\frac{z}{\mu})\right]. \tag{2.44}$$

By requiring that the integral of the limiting counterion distribution Eq. (2.40) vanishes, one can solve that $\Lambda_c^1 = -3/8$ in the exact $\kappa\mu = 0$ limit, so that the density itself approaches

$$\rho_c(z) \xrightarrow{\kappa\mu\to 0} [\frac{3}{8}(z/\mu - 1) + \frac{1}{2\Xi}([\frac{z}{\mu}]^2 - 2\frac{z}{\mu})]e^{-z/\mu}. \tag{2.45}$$

Here it is worth to emphasize that our formalism does not reproduce the same first-order correction to counterion density as the original SC formalism [51]. On top of the correction term $\frac{1}{2\Xi}([\frac{z}{\mu}]^2 - 2\frac{z}{\mu})$ we obtain a contribution arising from the $\phi^2$-term, describing the interaction between *artificial DH salt* and wall. This does not mean that our theory would be in contradiction with that of Netz, but instead our theory does not correctly describe the $\kappa\mu = 0$ limit, because we have already assumed in the derivation that bulk salt is weakly coupled, as was explained in the beginning of Sec. 2.1. Setting $\kappa\mu \to 0$ would force the bulk salt to be strongly coupled, and that is in contradiction with the assumptions.

Moreover, this DH salt term arising in this artificial limit of $\kappa\mu \to 0$ is not perturbative in $1/\Xi$, but is of the same order as the zeroth order result, giving the most significant contribution to first order ion densities. By comparing Eq. (2.45) to the leading order counterion density Eq. (2.29), we get a criterion for the validity of this expansion

$$z/\mu \ll \frac{11}{3}, \tag{2.46}$$

being much more restrictive than the criterion predicted by the SC theory, i.e., $z/\mu \ll \Xi^{1/2}$.

From the final density expressions it is also seen that the contribution arising from the DH interaction decreases the positive ion densities close to the wall compared to the zero salt case, but increases the negative ion density. The decrease is strongest for multivalent positive ions, typically the counterions with valence $q_c$ much larger than the valence of salt ions. This means that we do not get overcharging in the artificial limit of $\kappa\mu \to 0$, but instead more negative ions close to the wall as compared to zeroth order densities.

The validity of the first order expansion for finite but small $\kappa\mu$ is obtained by comparing the next-leading ion densities to the leading order one, i.e.

$$|\rho_\alpha^1| \ll |\rho_\alpha^0|, \tag{2.47}$$

which translates such that what is inside the curly brackets in Eqs. (2.37), (2.38) and (2.39), needs to be much smaller than unity. Because of the complexity of the equations, we only compare the lowest-order terms in $\kappa\mu$ from Eqs. (2.37), (2.38) and (2.39) to the leading-order densities Eqs. (2.20) and (2.21).

In the limit $\Xi \to \infty$ to the first order in $\kappa\mu$, we get

$$\rho_c^1(z) = \frac{1}{\Xi} e^{-z/\mu}\{(\frac{1}{2}z^2 - z/\mu) - \kappa\mu([\frac{z}{\mu}]^2 + z/\mu + 1)\} + \frac{3q_\alpha \Xi}{8q_c}(z/\mu - 1) + \mathcal{O}([\kappa\mu]^2). \tag{2.48}$$

This shows once more that in the artificial limit $\kappa\mu \to 0$, we do not get exactly the zero-salt results of Netz to the first order, but instead we have a large correction term arising from ion correlations between reservoir counterions and wall, being of the same order of magnitude in $\Xi$ as the zeroth order density. In addition, Eq. (2.48) shows that the meaning of ion-ion correlations is to decrease the ion densities close to the wall compared to the counterion only case calculated by Netz et al. [51], and increase them in bulk.

Based on these results, we can conclude that our formalism does not correctly reproduce the $\kappa\mu \to 0$ limit, because the approximations done in Articles I and II in the derivation of the theory force the bulk salt to be weakly coupled to the wall, and we should carry out the resummation of all the terms in the virial expanded partition function to make

the formalism work right. However, the result that the zeroth order density of our theory agrees with that of Netz's SC theory, suggests that some kind of a variational method applied for the salt ions might have a well-defined zero salt limit. However, this work is outside the scope of this Thesis, and will be carried out in the future.

### (ii) Strong Coupling with Weak Salt limit: Overcharging?

Here we introduce a regime that is important while considering the phenomena of overcharging. In this regime, it turns out that only multivalent ions are strongly coupled to the wall, but salt ions become decoupled from the wall. This means that *in the SC-DH limit, the assumptions used in the derivation of the theory become justified*. Due to the fact that in the SC theory the first layer already neutralizes the wall, the second layer of ions does not feel a strong interaction with the wall. However, since the first order density is mainly responsible for the formation of the "second layer", all the ions in the second layer are still strongly coupled to the "first layer" of atoms, and to all the neighboring atoms.

To put this idea into mathematical form, we use the approximation that the single particle interaction energy with the wall in Eq. (2.19)

$$e^{-\kappa z}/\kappa\mu \ll 1. \tag{2.49}$$

Because the minimum distance between the ions in the second layer and the wall is two times the ion radius $2a$, the criterion Eq. (2.49) in fact translates to

$$e^{-\kappa 2a}/\kappa\mu \ll 1. \tag{2.50}$$

Furthermore, we assume that the interaction between the ions is large even when it is described using the DH potential energy. This gives a *criterion for the validity* of the decoupling regime, and at the same time for the *whole SC-DH theory* used in this Thesis as

$$q_c q_- \frac{l_B}{2a} e^{-\kappa 2a} \gg 1, \text{ together with } \quad e^{-\kappa 2a}/\kappa\mu \ll 1, \tag{2.51}$$

where we have assumed that $q_c$ is the largest valence of the positive ions. This, as a consequence, gives a minimum requirement for the decoupling regime as

$$\frac{2a}{q_{\pm}^2 l_B} \ll \kappa\mu, \tag{2.52}$$

which is opposite to the criterion obtained in the zero-salt limit of Eq. (2.42). Thus, Eq. (2.52) seems to *set the lower limit of the validity of our SC-DH expansion*. The decoupling approximations (2.50) and (2.51) mean that the ions in the second layer are weakly coupled to the wall, but strongly coupled to the other ions, especially to ions in the first layer.

The interaction integral in Eq. (2.34) between the ion species can be written in this limit as

$$I_{\alpha,\beta}(z) = \frac{\rho_\alpha^0(\infty)}{q_c^2 l_B^2}[g1_{\pm}(z, 2a, q_\alpha, q_\beta) + \frac{q_\alpha l_B}{\kappa^2\mu} g2(z, 2a, q_\alpha, q_\beta)] + \frac{1}{6}\rho_\alpha^0(\infty) z^3, \tag{2.53}$$

where we have defined the auxiliary functions

$$\begin{aligned} g2(z, 2a, q_\alpha, q_\beta) = &\left[z^3 e^{+\kappa z + q_\alpha q_\beta l_B/z} - (2a)^3 e^{+\kappa 2a + q_\alpha q_\beta l_B/2a}\right]|_{z\geq 2a} \\ &+ (2a)^3 e^{-\kappa 2a + q_\alpha q_\beta l_B/(2a)}, \end{aligned} \tag{2.54}$$

and

$$g1_{\pm}(z, 2a, q_\alpha, q_\beta) = \left[(2a) e^{\pm q_\alpha q_\beta l_B/2a} - z^5 e^{\pm q_\alpha q_\beta l_B/z}\right]|_{z\geq 2a}. \tag{2.55}$$

By applying these results to the ion densities, we obtain the counterion density as

$$\begin{aligned} \rho_c^1(z) = \rho_c^0(z) \Bigg\{ &\Lambda_c^1/\Lambda_c^0 + 2\pi\frac{1}{2}\left[\Lambda_c^0 e^{-1/\kappa\mu} + \Lambda_+^0 e^{-q_+/q_c\kappa\mu} + \Lambda_c^- e^{+q_-/q_c\kappa\mu}\right]\frac{z^3}{3} \\ &+2\pi\frac{q_-\Lambda_-^0 e^{+q_-/q_c\kappa\mu}}{q_- q_c^2 l_B^2} g1_+(z, 2a, q_c, q_-) - 2\pi\frac{q_+\Lambda_+^0 e^{-q_+/q_c\kappa\mu}}{q_+ q_c^2 l_B^2} g1_-(z, 2a, q_c, q_+) \\ &-2\pi\frac{q_c\Lambda_c^0 e^{-1/\kappa\mu}}{q_c^3 l_B^2} g1_-(z, 2a, q_c, q_c) - \frac{\kappa^2}{4l_B} I_{DH}(q_c, z)\Bigg\}. \end{aligned} \tag{2.56}$$

This means that the contribution arising from interactions to ion density is large only for $z \geq 2a$, since the $z^3$ and $I_{DH}(q_c, z)$ terms are small compared to zeroth order density, and also much smaller than ion-ion interaction terms described by using $g_\alpha$ functions. This

is the same as saying that first order density contributions become important only in the *second layer of atoms*.

In the same way we also find the salt ion densities as

$$\rho_+^1(z) = \rho_+^0(z)\left\{\frac{\Lambda_+^1}{\Lambda_+^0} + 2\pi\frac{1}{2}\left[\Lambda_c^0 e^{-1/\kappa\mu} + \Lambda_+^0 e^{-q_+/q_c\kappa\mu} + \Lambda_c^- e^{+q_-/q_c\kappa\mu}\right]\frac{z^3}{3}\right.$$
$$+2\pi\frac{q_-\Lambda_-^0 e^{+q_-/q_c\kappa\mu}}{q_- q_c^2 l_B^2} g1_+(z,2a,q_+,q_-) - 2\pi\frac{q_+\Lambda_+^0 e^{-q_+/q_c\kappa\mu}}{q_+ q_c^2 l_B^2} g1_-(z,2a,q_+,q_+) \quad (2.57)$$
$$\left.-2\pi\frac{q_c\Lambda_c^0 e^{-1/\kappa\mu}}{q_c^3 l_B^2} g1_-(z,2a,q_+,q_c) - \frac{\kappa^2}{4l_B} I_{DH}(q_+,z)\right\},$$

and

$$\rho_-^1(z) = \rho_-^0(z)\left\{\frac{\Lambda_-^1}{\Lambda_-^0} + 2\pi\frac{1}{2}\left[\Lambda_c^0 e^{-1/\kappa\mu} + \Lambda_+^0 e^{-q_+/q_c\kappa\mu} + \Lambda_c^- e^{+q_-/q_c\kappa\mu}\right]\frac{z^3}{3}\right.$$
$$+2\pi\frac{q_-\Lambda_-^0 e^{+q_-/q_c\kappa\mu}}{q_- q_c^3 l_B^2} g1_-(z,2a,q_-,q_-) - 2\pi\frac{q_+\Lambda_+^0 e^{-q_+/q_c\kappa\mu}}{q_+ q_c^3 l_B^2} g1_+(z,2a,q_-,q_+) \quad (2.58)$$
$$\left.-2\pi\frac{q_c\Lambda_c^0 e^{-1/\kappa\mu}}{q_c^3 l_B^2} g_+(z,2a,q_-,q_c) - \frac{\kappa^2}{4l_B} I_{DH}(q_-,z)\right\}.$$

In the regime of validity of Eq. (2.52) the terms depending on $g1_\pm$ dominate over the ones depending on $g2$, for $z > a_\perp/(q_c\kappa\mu)$. In the case $2a > a_\perp/(q_c\kappa\mu)$ this criterion holds in the second layer, meaning that $g1_\pm$ gives the dominant contribution to densities.

From these mathematical considerations, and especially from the approximations to final ion densities of Eqs. (2.56), (2.57) and (2.58), one can figure out the physical mechanism behind *overcharging*. If we neglect the positive salt ions for a moment, we can make this more understandable. The most dominant term in the first order counterion density Eq. (2.56) is the interaction term $I_{DH}(q_-,z)$ with the negative ions depending on the $g1_+$-function, and having a prefactor equal to the zeroth order bulk charge density of negative salt ions. In the same way, the largest contribution to the negative ion-density Eq. (2.58) comes from the interaction integral with counterions and depends also on the function $g1_+$, but having a prefactor equal to the zeroth order bulk charge density of counterions, or surplus of counterions not needed for the neutralization of the charged wall. Due to the bulk electroneutrality of zeroth order, the prefactors are almost identical differing only by

a constant, being $1/q_-$ for counterions and $1/q_c$ for negative ions. This has a very simple physical interpretation. In the second layer of ions, all the negative ions stick to positive ions in the first layer, whereas positive ions in the second layer stick to negative ions in the first layer. According to the SC theory, it is already the first layer of ions that makes the surface electroneutral, or more precisely both surface and bulk electroneutral, since all the normalization equations separate into bulk and surface parts, see Sec. 2.1. This has the consequence that the second layer has a charge equal to

$$Q^1 = q_c N_-^0 - q_- N_c^0, \tag{2.59}$$

where $N_c$ and $N_-$ are the number of bulk counterions and bulk negative ions in the first layer, respectively. Due to the electroneutrality of the first layer we have the relation $q_- N_- = q_c N_c$. By inserting this into Eq. (2.59), one can write the total amount of charge in the second layer as

$$Q^1 = q_c N_-^0 - \frac{q_-^2}{q_c} N_-^0 \equiv (q_c^2 - q_-^2) N_-^0 / q_c > 0, \tag{2.60}$$

if $q_c > q_-$, which is the case in the SC limit, meaning that we obtain *overcharging or positive apparent surface charge* at certain distances from the wall. By developing the same idea as here, one can easily see that the *third layer of ions is negative*, but the charge of the third layer is actually smaller than the charge in the second layer, meaning that the overall charge of the first, second and third layer is still positive. This reasoning can be continued for layers more distant from the wall, such that finally the sum of all ion layers is zero. Using the same logic, one can argue that the maximum of the integrated charge happens exactly at the distance $z = 4a$.

Now we could give the approximate solution to the normalization Eqs. (2.17) in the SC-DH regime, but these expressions are not very instructive. Instead we show plots of the full second order ion densities solved numerically for different $\kappa\mu$ in Fig. 2.3, and also the integrated charge, or *apparent surface charge*, in Figs. 2.2 defined as

$$Q_{int}(z) = -\sigma_s \pm \sum_\alpha q_\alpha \int_0^z \mathrm{d}x \rho_\alpha(x), \tag{2.61}$$

where all the ion densities are given by the second order result in virial limit, i.e., Eqs. (2.14) and (2.15). On top of the bulk salt concentration $\kappa\mu$, these all depend basically on 6 relevant parameters: ion radius $a$, counterion valence $q_c$, positive salt and negative salt ion valences $q_\pm$, surface charge density $\sigma$, and $l_B$. Since we are mainly interested in the SC limit where $\Xi \to \infty$, we fix the surface charge density to a large but physically reasonable value $\sigma_s = 0.095\text{nm}^{-2}$, and use the Bjerrum length of water, which is $l_B = 0.71$ nm.

In Figs. 2.2 we show the integrated charge as a function of the salt concentration for fixed valences and ion radius. The most dramatic conclusion is that for fixed $z$, the *integrated charge is a non-monotonic function of* $\kappa\mu$. For small but finite $\kappa\mu$, the integrated charge increases when bulk salt is increased. However, for each set of parameters our numerical results predict that for very large values of $\kappa\mu \geq 1$, it finally turns to a decreasing function. This means that there has to be a crossover value of $\kappa\mu$, where the physically interesting overcharging seems to take place.

In Fig. 2.2(d), we show the integrated charge for a fixed ion radius and bulk salt concentration, but varying valence of counterions. Here it is also assumed that bulk salt is monovalent, i.e. $q_\pm = 1$. It is seen that for fixed $a$ and $\kappa\mu$ the integrated charge is a monotonically increasing function of $q_c$. For $\{a = 0.5\text{Å}, \kappa\mu = 0.5\}$, we see that the integrated charge is greatly amplified when $q_c$ varies between $\{2, 10\}$. When $q_c = 2$, one does not see overcharging, whereas for $q_c = 4$ and $q_c = 10$ there is a clear overcharging. For the case $\{a = 2\text{Å}, \kappa\mu = 0.1\}$ the maximum of the integrated charge increases as a function of $q_c$, too, but here only the case $q_c = 10$ is overcharged, and by only a few per cent. In case $\{a = 0.5\text{Å}, \kappa\mu = 0.5\}$, it is seen that the magnitude of the integrated charge depends also on $z$, and for $z \leq 2$Å the integrated charge is larger for $q_c \in \{2, 4\}$, compared to $q_c = 10$, whereas for larger values of $z$ the situation is reversed. Altogether, this shows that the contribution of counterion valence to integrated charge depends on the ion radius, bulk salt concentration and especially on the distance from the wall $z$.

In Figs. 2.3 and 2.4 we show the first order total positive ion densities $\rho_c^1/\rho_c^0(z) + \rho_+^1/\rho_+^0(z)$

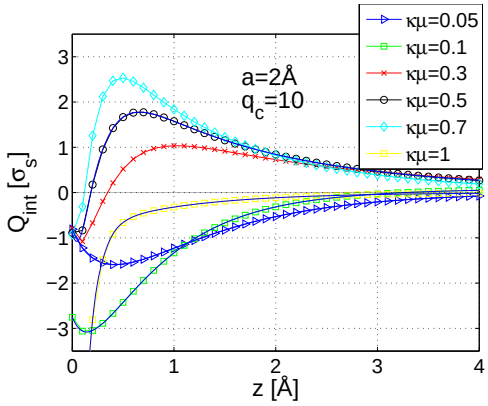


(a) $a = 2, q_c = 10$

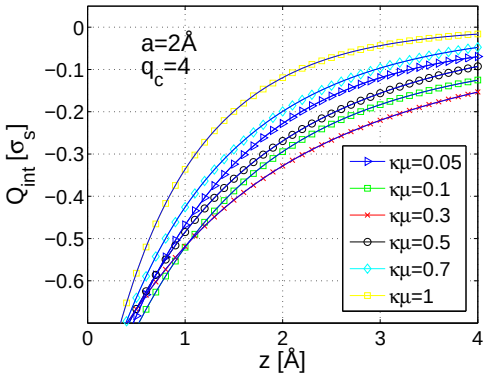


(b) $a = 2, q_c = 4$

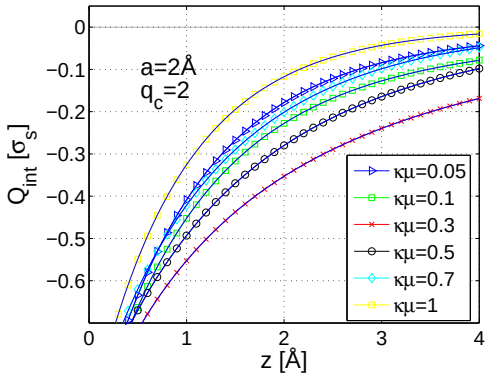


(c) $a = 0.5, q_c = 2$

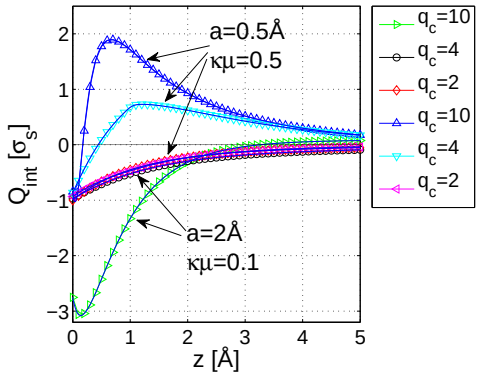


(d) Combinations ($a = 2, \kappa\mu = 0.1$) and ($a = 0.5, \kappa\mu = 0.5$), with varying $q_c$.

**Figure 2.2**: Integrated charge for different counterion valences. (a) $q_c = 10$, (b) $q_c = 4$, (c) $q_c = 2$, (d) Integrated charge for fixed salt concentration and ion radius, but varying counterion valence.

and negative salt ion densities $\rho_-^1/\rho_-^0(z)$ that are normalized by the zeroth-order ion densities. All the ion densities behave very similarly to the integrated charge itself, since the total integrated charge is nothing but the sum of all the charges. However, for small $a$ or large $q_c$ it seems that the first-order ion densities become larger than the zeroth order ion densities, implicating the breakdown of the whole theory. Mathematically the SC theory breaks down for those values of $z$ for which the normalized first-order densities exceed unity in Figs. 2.3 and 2.4. However, it is also seen that for all salt concentrations the normalized ion densities approach zero quickly. Even in the worst case of $\{q_c = 10, a = 2\text{Å}\}$ the normalized ion densities are smaller than unity already for $z > 2\text{Å}$, obeying the criterion of the validity of the SC expansion Eq. (2.47). It is also seen from Fig. 2.3 that for parameters $\{q_c = 2, a = 2\text{Å}\}$ the normalized ion-densities are much smaller than unity, thus satisfying the SC criterion Eq. (2.47) for all $\kappa\mu$ and for all $z$.

The breakdown of the SC expansion for small ion radii does not seem problematic for the realistic applications. In water the small positive (negative) ions create a hydration shell around them, such that for example hydrogen ion $H^+$ appears as a hydronium $H_3O^+$ in water, and lithium shows up together with its four hydrated water molecules. These ion-complexes have a size exceeding $0.5\text{Å}$ at least by a factor of $2$, by comparing to the diameter of the hydronium molecule being roughly $1\text{Å}$. Moreover, the more charged the ion is, the bigger it is on average, and the larger the hydration shell. By comparing the ion densities for $q_c = 4$ with varying ion radius in Figs. 2.5, 2.6, it is observed that the absolute value of the ion densities decays by a factor between $10$ and $100$, when the ion radius is increased from $a = 0.5\text{Å}$ to $a = 1\text{Å}$, but changes only slightly from $1\text{Å}$ to $4\text{Å}$, see Figs. 2.5 and 2.6. This certainly means, that the results predicted by the theory are wrong in the case $\{a = 0.5\text{Å}, \kappa\mu = 0.1\}$, see Figs. 2.5(a) and 2.6(a). The case $\{a = 0.5\text{Å}, \kappa\mu = 0.5\}$ seems to be a borderline, since even the normalized positive ion density exceeds unity only for the first two data points in Figs. 2.5(b) and 2.6(b), i.e. for very short distances from the wall. However, in case $\{a = 0.5\text{Å}, \kappa\mu = 1\}$, the results shown in Figs. 2.5(c) and 2.6(c) are valid for all distances $z$ from the charged wall. This highlights the fact that it is a combination of $a$, $\kappa\mu$ and $\Xi$ that sets the limit to the validty

of our theory, see Eq. (2.52).

These results reveal that one cannot talk about the SC expansion only in terms of $\Xi$, but that also the ion radius $a$ as well as the bulk salt concentration $\kappa\mu$ play a big role. Since the ion-ion correlations show up through the second virial coefficient, they strongly depend on the exponential of $l_B/2a \propto \Xi/\tilde{a}$. This means that while the ion densities become smaller at large distances from the charged wall for increasing $\Xi$, they are also magnified at small distances through the Mayer-function interactions. However, as was explained before, the realistic ion radius together with its hydration shell typically exceeds 1Å, meaning that the theory becomes rather indipendent of the hardcore radius chosen.

### (iii) Excess salt limit

It is shown in Article II of this Thesis that in the limit $q_c^2 l_B e^{-\kappa 2a}/2a \ll 1$ the Mayer functions can be re-expanded as $1 - e^{\mp v_{DH}(\mathbf{r})} = \pm v_{DH}(\mathbf{r}) \approx \frac{\Xi}{(\kappa\mu)^2}\delta(\mathbf{r})$. This typically happens only under conditions of excess salt, such as 1M of sodium chloride, corresponding to $\kappa^{-1} \approx 3.3\text{nm}^{-1}$, but clearly depends also on $a$ and $l_B$. It is even more important to realize that the criterion for this to happen is

$$\frac{(\kappa\mu)^2}{\Xi} \gg 1. \tag{2.62}$$

To put this into more formal language, let us expand the interaction terms in first order ion densities as

$$I = \int \mathrm{d}\mathbf{r}' \rho_\alpha(\mathbf{r}')[1 - e^{\mp q_\alpha q_\beta v_{DH}(\mathbf{r}-\mathbf{r})}] \to \pm \frac{q_\alpha q_\beta l_B}{\kappa^2}\rho_\alpha(\infty)e^{-\kappa z}, \tag{2.63}$$

which immediately implies that for the first order ion densities we get a simple expression

$$\begin{aligned}\rho_\alpha^1(z) &= \rho_\alpha^0(z)\left[\frac{\Lambda_\alpha^1}{\Lambda_\alpha^0} - \frac{\kappa^2}{4l_B}I_{DH}(q_\alpha, z) \pm \frac{l_B}{\kappa^2}(q_-\rho_-^0(\infty) - q_+\rho_+^0(\infty) - q_c\rho_c^0(\infty))e^{-\kappa z}\right] \\ &\equiv \rho_\alpha^0(z)\left[\Lambda_\alpha^1 - \frac{\kappa^2}{4l_B}I_{DH}(q_\alpha, z)\right],\end{aligned} \tag{2.64}$$

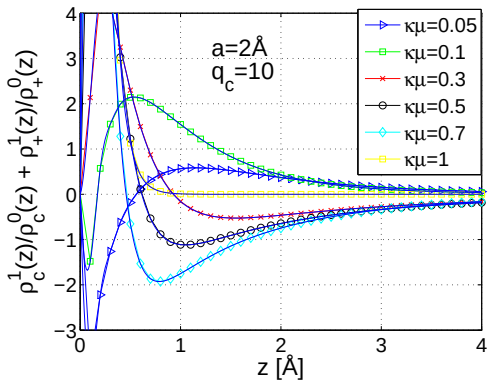


(a) $a = 2\text{Å}, q_c = 10$

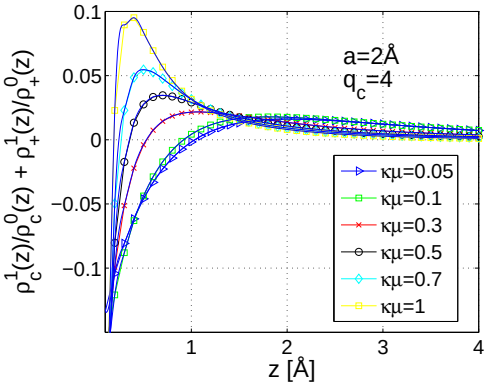


(b) $a = 2\text{Å}, q_c = 4$

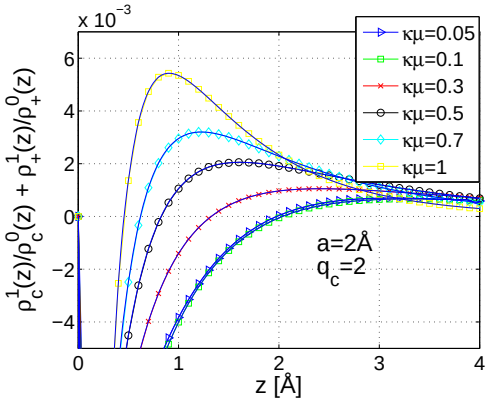


(c) $a = 0.5\text{Å}, q_c = 2$

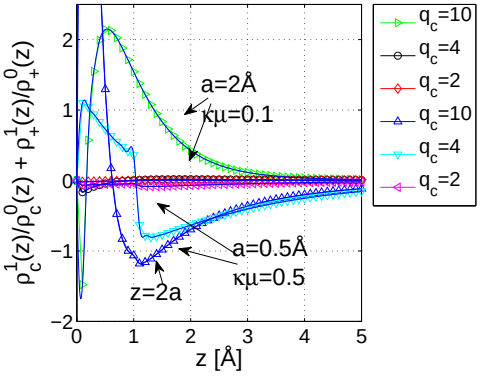


(d) Combinations $\{a = 2\text{Å}, \kappa\mu = 0.1\}$ and $\{a = 0.5\text{Å}, \kappa\mu = 0.5\}$, with varying $q_c$.

**Figure 2.3**: Normalized positive ion density for different counterion valences. (a) $q_c = 10$, (b) $q_c = 4$ , (c) $q_c = 2$, (d) Normalized positive ion density for fixed salt concentration and ion radius, but varying counterion valence.

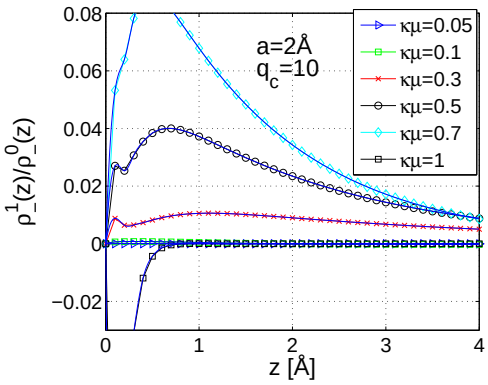


(a) $a = 2, q_c = 10$

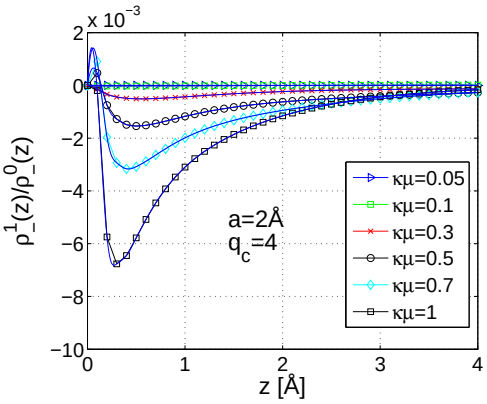


(b) $a = 2, q_c = 4$

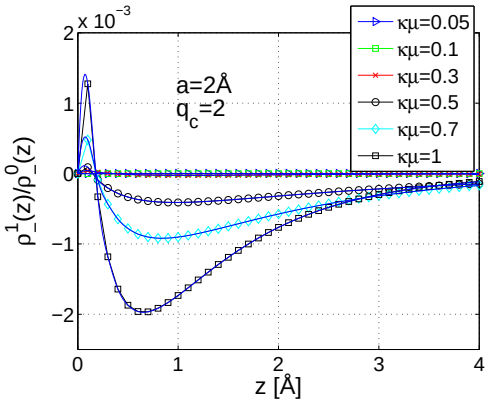


(c) $a = 0.5, q_c = 2$

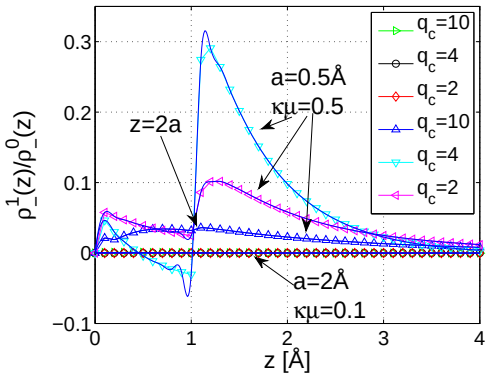


(d) Combinations ($a = 2, \kappa\mu = 0.1$) and ($\{a = 0.5, \kappa\mu = 0.5\}$), with varying $q_c$.

**Figure 2.4**: Normalized negative ion density for different counterion valences. (a) $q_c = 10$, (b) $q_c = 4$ , (c) $q_c = 2$, (d) Normalized negative ion density for fixed salt concentration and ion-radius, but varying counterion valence.

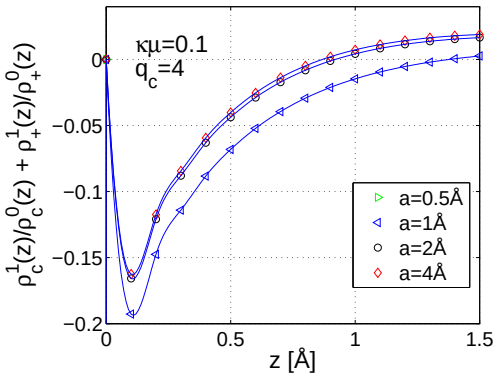


(a) $\kappa\mu = 0.1$

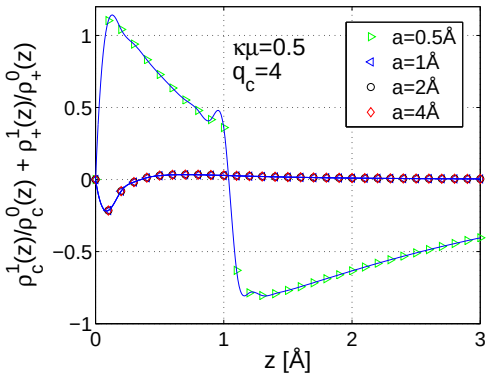


(b) $\kappa\mu = 0.5$

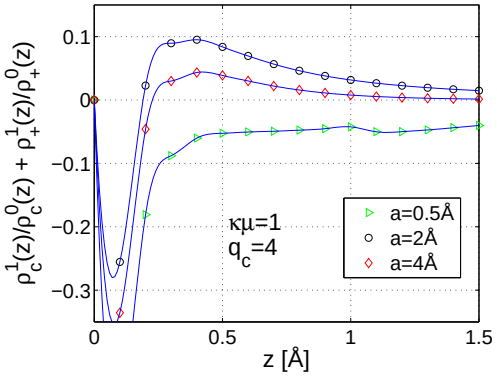


(c) $\kappa\mu = 1$

**Figure 2.5**: Normalized positive ion density for different ion radii. Counterion valence is fixed to $q_c = 4$, and the added salt is monovalent in all cases, i.e. $q_+ = q_- = 1$. The "jump" in the ion densities that takes place at $z = 2a$, is due to the lack of enough data points. Positive ion densities decrease strongly after $z = 2a$, but they are continuous functions of $z$.

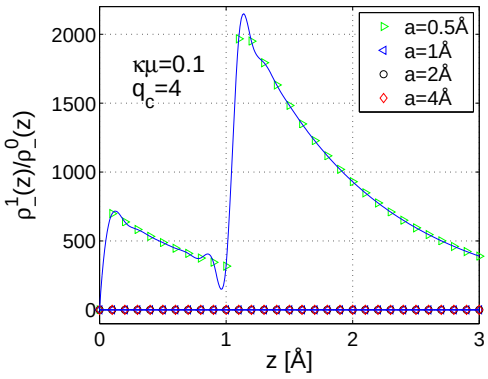


(a) $\kappa\mu = 0.1$

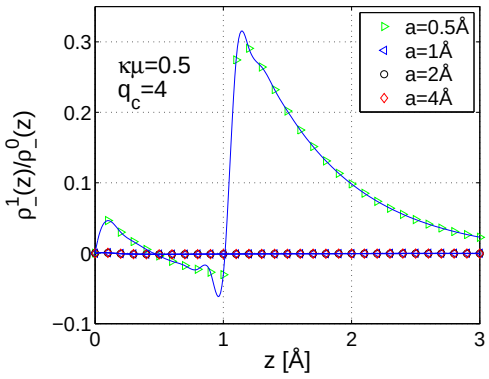


(b) $\kappa\mu = 0.5$

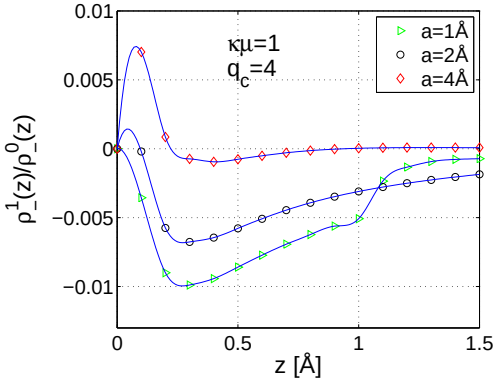


(c) $\kappa\mu = 1$

**Figure 2.6**: Normalized negative ion density for different ion radii. Counterion valence is fixed to $q_c = 4$, and the added salt is monovalent in all cases, i.e. $q_+ = q_- = 1$. The "jump" in the ion densities that takes place at $z = 2a$, is due to the lack of enough data points. Negative ion densities increase strongly after $z = 2a$, but they are continuous functions of $z$.

where the last equality follows from the electroneutrality of the zeroth order densities.

In this limit the zeroth order ion densities read as

$$\rho_\alpha(z) = \rho_\alpha^0(\infty)[1 \pm \frac{q_\alpha}{q_c \kappa\mu} e^{-\kappa z}]. \tag{2.65}$$

This result, in fact, is the same as the leading order counterion density in the DH limit, i.e. in the presence of excess salt. However, one should not believe that we have obtained the DH limit rigorously, because these two theories have their own regimes of applicability, namely given by the next-leading density term.

By plugging Eq. (2.65) into the first order density expression Eq. (2.64) we can easily work out the normalization integrals in Eq. (2.17). The first order fugacities obtained this way are

$$\begin{aligned}
\Lambda_c^1 &= -\frac{1}{8q_c}\frac{[q_c\Lambda_c^0 + q_+^2\Lambda_+^0/q_c + q_-^2\Lambda_-^0/q_c]}{[q_+ + q_-[q_+/q_-]^2]}; \\
\Lambda_+^1 &= \frac{1}{8}\frac{[q_c\Lambda_c^0 + q_+^2\Lambda_+^0/q_c + q_-^2\Lambda_-^0/q_c]}{[q_+ + q_-[q_+/q_-]^2]}; \\
\Lambda_-^1 &= -\frac{1}{8}\frac{[q_c\Lambda_c^0 + q_+^2\Lambda_+^0/q_c + q_-^2\Lambda_-^0/q_c]}{[q_+ + q_-[q_+/q_-]^2]},
\end{aligned} \tag{2.66}$$

where $\Lambda_\alpha^0$ are given by Eqs. (2.24), (2.25) and (2.26). This shows that in the excess salt limit the first order correction to ion densities is of the same order of magnitude in $\Xi$ and $\kappa\mu$ than zeroth order. However, the numerical prefactor in front of the fugacity is about one order of magnitude smaller, implying that this expansion is converging. Finally we can write the first order ion densities in the excess salt limit as

$$\rho_\alpha(z) = \rho_\alpha^0(\infty)\Lambda_\alpha^1/\Lambda_\alpha^0 \pm \frac{q_\alpha\rho_\alpha^0(\infty)}{q_c\kappa\mu} e^{-\kappa z}[\Lambda_\alpha^1/\Lambda_\alpha^0 + \frac{1}{4}\kappa z - \frac{1}{8}]. \tag{2.67}$$

Furthermore, if we count the next order in ion-ion interaction terms, we get terms of order $\Xi/(\kappa\mu)^2$, in agreement with the criterion Eq. (2.62). These results mean that *in the excess salt limit the SC-DH theory becomes valid for all values of* $z$.

## 2.2 Conclusions and Summary

In Articles I and II of this Thesis, we have derived a general field theory for both counterion and coion distributions around an arbitrary macroscopic charged object. This theory assumes implicitly that bulk salt ions are electrostatically weakly coupled to the charged wall, whereas the counterions are strongly coupled. Thus, in the limit of an excess amount of bulk salt, our theory becomes exact. Mathematically the assumption about weakly coupled salt shows up in the field-theoretic propagator that is assumed to be of the DH form.

In Article I we calculated the zeroth-order ion densities, and analyzed that case completely. One of the main results was that our theory has a smooth limit $\kappa\mu \to 0$ to the SC theory of Netz [51]. In Article II we considered the first order correction to this theory via a second order virial coefficient. Here it turns out that the bulk salt ion correlations with counterions give a significant contribution to counterion density being of the same order of magnitude in $\Xi$ than the zeroth order ion densities. In the exact $\kappa\mu \to 0$ limit this theory becomes incorrect, giving right predictions only at very small distances from the charged wall. However, in the opposite limit of $\kappa\mu \to \infty$, our theory becomes exact, and as it was shown in Article II, to the leading order it gives the same results as the DH theory. The lack of the proper zero-salt limit of our theory is due to the perturbative subtraction of the exponential of the $\phi^2$ terms in the grand-canonical partition function. In the limit $\kappa\mu \to 0$, these terms become the dominant ones, thus invalidating the assumption that $\phi^2$ is small.

By expanding around the excess salt limit, we can also interpolate to the finite values of $\kappa\mu$. Most interestingly, we can show that at certain regime of bulk salt concentration described by Eq. (2.51), one observes the formation of ion layers that is a combination of both finite ion size and the strong attraction between oppositely charged ions. It is also argued that this layer formation seems to be the physical reason behind overcharging. One of the consequences of this interpretation of overcharging is that the maximum of the integrated charge should be at the distance of two ion diameters from the wall, which

is in agreement not only with our numerical findings, but also with recent simulation results for strongly charged colloidal particles [38, 45–47].

To demonstrate the usefulness of our formalism, we have obtained explicit results for the case of a single charged plate in the presence of counterions and a finite concentration of bulk salt. The main results are the density distributions for all ion types as a function of the distance from the plates. As a consequence, we also calculated the total integrated charge as a function of distance, sometimes called apparent surface charge. Our results reveal that for a certain distance from the wall and for a limited regime of bulk salt, the integrated charge changes sign from negative to positive, and we obtain what is called *charge inversion* or *overcharging* [38, 39, 47, 62, 67, 69].

The magnitude of overcharging, as well as the magnitude of first order ion densities, depend non-monotonically on bulk salt concentrations $\kappa\mu$, but increases monotonically as a function of counterion valence. By explicitly calculating the ion-densities in the ill defined $\kappa\mu \to 0$ limit, we see that overcharging always vanishes, and total charge density is decreased close to a charged wall. Furthermore, in the excess salt limit we find agreement with the DH theory, showing that overcharging is a decreasing function of the bulk salt $\kappa\mu$. Our numerical solutions for first order ion densities reveal that for ion radii smaller than or equal to $0.5$Å, the ion densities increase strongly giving results not consistent with the assumptions of our theory. However, for an ion radius larger or equal to $1$Å, the ion densities are by and large insensitive to the magnitude of the ion radius, as one might assume based on quantum mechanical considerations. However, the larger the counterion valence is, the larger the radius of the ion should be for the SC expansion to be convergent.

# 3 DNA Overstretching Transition: Ionic Strength Effects

In this Chapter we extend our goal of considering charged biomolecules to concern not only electrostatic degrees of freedom as in Sec. 2, but also elastic and internal degrees of freedom. The motivation to do this is to consider a structural phase transition that takes place when DNA is stretched from one end with certain force by using for example atomic force microscopy or optical tweezers. Due to the recent development of these single-molecule manipulation techniques [8, 73], it is nowadays possible to study elastic properties of DNA, and its stability against force-induced overstretching transition, or B-to-S transition. These studies all focus on how double-stranded B-DNA is stretched and bend, and how, at some critical force of approximately 70 pN, it will give way to a new conformation, here for simplicity denoted as S-DNA.

The nature of force-induced denaturation of DNA puts severe constraints on theoretical modeling: the passage from B-DNA to S-DNA involves mesoscopic elastic deformations as well as more localized processes, notably breaking of base pairs. A reasonable overstretching and denaturation model must, therefore, contain two distinct, but coupled, sets of state variables for elasticity and breaking of base pairs, respectively.

Traditionally one describes DNA as a semiflexible polymer chain, being a one-dimensional solid object that can be stretched, bent or twisted. If DNA is also stretched by external force from one end, one can describe it in the rod-like limit, showing only small temperature fluctuations around straight configuration. The free energy of this semiflexible rod-like polymer is reviewed in Sec. 3.1.

On top of the elastic degrees of freedom, DNA has also internal structure. DNA is composed of two single strands coupled together into double helix by hydrogen bonds

between the bases in opposite strands. Being a highly nonlinear many-body quantum mechanical problem, the hydrogen bonding cannot be put into our statistical mechanics model microscopically, but one has to resort to a phenomenological description. Here we take a point of view that DNA is composed of domains of base pairs being either bonded to each other or separated. These domains are then separated by artificial junctions, which are energetically unfavorable. It can be shown that this kind of description leads to an Ising model, where the spin variables present the junctions. This description was first introduced by Cluzel et al. [10].

Models along these lines to describe the B-to-S transition have been proposed by Ahsan et al., Rouzina et al. [1, 63], and more recently by Metzler et al. [20]. Ahsan et al. [1] proposed a faithful model of denaturation (Ising-type), which is coupled to the mesoscopic elastic degrees of freedom in an elegant way, and which also seems very appealing for introducing salt into the description. However, all these existing models of the B-to-S transition have ignored the salt dependence of this transformation, which raises at least two interesting questions. *First*, one wonders if the electrostatic component of the B-to-S transition is already taken into account by the mesoscopic elasticity, or whether other (local or global) effects are involved. *Secondly*, one can ask how well the data conform to the much invoked Manning condensation theory [42], which predicts the effective separation between charges along DNA-chain after condensation has taken place.

In what follows, I will briefly present our hybrid model which combines the Ising-model approach of Ahsan et al. [1] and the elasticity theory by Podgornik et al. [56]. A statistical mechanics analysis of the hybrid model allows us to compute force-extension curves which depend on (phenomenological) electrostatic, Ising, and elastic parameters, and which fit the experimental data by Wenner et al. [70] very well.

## 3.1 DNA Elasticity

Mechanical properties such as bending, stretching and twisting and their respective elastic moduli determine conformations of DNA in mesoscale. In the terminology of physics, DNA is a semiflexible charged polymer or polyelectrolyte. Polyelectrolytes, a class of polymers, are charged macromolecules, which contain a large number of watersoluble ionizable ionic groups. In solutions polyelectrolytes show up with neutralizing, diffusing counterions. In the presence of bulk salt, counterions and bulk salt ions partly screen the electrostatic interaction between the monomers, as was seen in Sec. 2. In the case of DNA, the negatively charged phosphate groups are responsible for its polyelectrolyte nature, and for non-zero salt concentrations we can think that these phosphate groups interact repulsively in the screened Coulombic interaction, i.e. DH interaction. In what follows, I present an elastic model for DNA in the rod-like limit, which is a natural starting point in the case of external stretching field.

### 3.1.1 Model for Semiflexible Chain

The starting point in presenting a theory for a self-interacting polymer chain is the formulation of the elastic mesoscopic Hamiltonian. It is assumed that in the limit of high external field, deformations away from the rodlike configurations are small. One should notice that also in the limit of vanishing bulk salt concentration the chain is rodlike, since the unscreened Coulomb interaction straightens the polyelectrolyte. Thus we consider a self-interacting chain in the highly stretched, small deformation limit in the Monge-like parametrization $\mathbf{r}(s) = (z, \rho(z))$, where $s$ is the arc length along the chain. The chain is described as a one-dimensional solid, so a sufficient representation is obtained by a deformation tensor with only one nonzero component, chosen to be in the $z$ direction

$$u_{zz} = \frac{\partial u_z(z)}{\partial z} + \frac{1}{2}\left(\frac{\partial \rho(z)}{\partial z}\right). \tag{3.1}$$

Here $u_z(z)$ is the internal phononlike field describing the stretching of the chain. The bending field $\rho(z)$ is in the direction perpendicular to the local tangent of the chain, thus $|\rho|$ is the radial distance from the $z$ axis. This result can be derived straightforwardly from the form of the line element along the chain: $\mathrm{d}s(z)^2 = [(\mathrm{d}z + \mathrm{d}u_z)^2 + (\mathrm{d}\rho(z)^2]$, leading to the lowest order in the deformation field to

$$\mathrm{d}s(z) = \mathrm{d}z \left[ 1 + \frac{\partial u_z(z)}{\partial z} + \frac{1}{2} \left( \frac{\partial \rho(z)}{\partial z} \right)^2 \right] + ... \tag{3.2}$$

By using Eq. (3.1) we can write the Hamiltonian of a self-interacting semiflexible chain as

$$\begin{aligned} \beta\mathcal{H}[\mathbf{r}] &= \beta\mathcal{H}_{el}[\mathbf{r}] + \beta\mathcal{H}_{stiff}[\mathbf{r}] + \beta\mathcal{H}_{int}[\mathbf{r}] \\ &= \frac{1}{2}\lambda \int \mathrm{d}s(z) \left[u_{zz}(z)\right]^2 + \frac{1}{2} K_C \int \mathrm{d}s(z) \left[ \frac{\partial^2 \rho(z)}{\partial z^2} \right]^2 \\ &+ \int \int \mathrm{d}s(z) \mathrm{d}s(z') v_{DH}(|\mathbf{r}(\mathbf{s}) - \mathbf{r}(\mathbf{s}')|) + \frac{1}{2} \int \mathrm{d}s(z) \dot{\mathbf{r}}(s) \cdot \mathbf{f}. \end{aligned} \tag{3.3}$$

Here $f$ is the external force stretching the chain in $z$ direction, $\lambda$ is the stretching modulus and $K_C$ is the bending modulus related to the persistence length $l_p$ as $K_C = k_B T l_p$ [23, 54]. The DH interaction potential has the usual form of $v_{DH}(\mathbf{r}) = l_B e^{-\kappa|\mathbf{r}|}/|\mathbf{r}|$, and $\kappa$ is the inverse Debye screening parameter defined in Eq. (2.7).

The free energy is now obtained by integrating over the fluctuating fields $u_z(s)$ and $\rho(z)$. However, straightforward integration does not work, due to the interaction potential which in general is not harmonic. One can resort to variational approximation [53], or the so-called $1/d$-expansion [23], $d$ being the dimension of the embedding space. In this way one obtains the approximate free energy that becomes correct on the largest scales. From such a formulation the equation of state, i.e. the force-extension relation, follows as

$$\frac{z}{L} = 1 - \frac{k_B T}{2\sqrt{K_C^R f}} + \frac{f}{\lambda^R}. \tag{3.4}$$

Here, instead of the original elastic constants, one obtains renormalized (shown by superscript $R$) elastic moduli. Their dependencies on the parameters in electrostatic potential

are given by the following relations [56]

$$\begin{aligned} \lambda^{(R)} &= \lambda - \frac{k_{\mathrm{B}}Tl_{\mathrm{B}}}{\Delta^2 c^2}(\mathrm{e}^{\kappa b} - \mathrm{Ei}(-\kappa b)), \\ K_C^{(R)} &= K_C + \frac{k_{\mathrm{B}}Tl_{\mathrm{B}}}{4\Delta^3(\kappa c)^2}, \end{aligned} \tag{3.5}$$

where $K_C$ and $\lambda$ are the bare values of elastic parameters corresponding to a limit of infinite concentration of salt, and $c$ ia the salt-renormalized separation between charges. In addition, $\mathrm{Ei}(x)$ is the standard exponential integral function and $\Delta$ is the local stretching parameter introduced as $\Delta = \left(\frac{\lambda+f}{\lambda^{(R)}}\right)$.

We can straightforwardly calculate the free energy $G_{\mathrm{el}}(f, L)$ of the chain related to the external force by $-\frac{\partial G_{\mathrm{el}}(f,L)}{\partial f} \equiv x$, which is the condition of mechanical equilibrium in a fixed force ensemble. This can be easily integrated to give

$$G_{\mathrm{el}}(f, L) = L\left[\frac{f^{1/2}}{\beta\sqrt{K_C^{(R)}}} - f - \frac{1}{2}\frac{f^2}{\lambda^{(R)}}\right] \equiv Lg(f), \tag{3.6}$$

where $\beta = 1/k_{\mathrm{B}}T$. Equation (3.6) provides the elastic free energy of a charged semiflexible chain under external force $f$. This expression for the free energy can be taken as a starting point when a model for the DNA overstretching transition is developed in Sec. 3.2.

## 3.2 Overstretching Transition

Sec. 3.1 described the properties and behavior of the semiflexible polymer chain under external force $f$, and showed how the elastic parameters are renormalized under the electrostatic interaction between the monomers. It also explained how the salt dependence on these parameters can be found in the regime of moderate extension. In this Section, our aim is to concentrate on the behavior of the DNA chain when the external force exceeds a limit where the internal structure of the chain starts to respond to this stretch.

It has been shown in many experiments [29, 37, 70, 73–75] that when a double-stranded DNA is stretched beyond its B-form contour length, it shows a highly cooperative overstretching transition. It seems that the DNA molecule abruptly increases its length by a factor between 1.5 and 2 when the external force $f$ exceeds a threshold in the range of $60-70$ pN. This phenomenon is recapitulated in Fig. 3.1. At this point the DNA molecule suddenly extends with little additional force. After this point, the force again rises rapidly with a slope that depends on the stretching rate [3, 70].

To describe the overstretching transition theoretically, one cannot use the simple elasticity theory presented in Sec. 3.1, since for large stretching forces the chain internal structure starts to break, and it does not respond linearly to increasing force. Instead, one needs to introduce artificial degrees of freedom to describe the hydrogen bonding of the two single strands. From the microscopic point of view, this would clearly require solving the quantum mechanical Schrödinger equation with all atoms included explicitly, but due to the number of atoms included into problem, this becomes impossible. A common classical approach first introduced by Cluzel et al. [10], is to use a *two-state model*, in which the DNA-chain is composed of interacting segments being either in the B-state or the S-state. The microscopic interpretation is that in the B-state there exists a bond between the bases in opposite single strands, and in the S-state this bond is broken. This kind of description leads to an *Ising model* for the *spin variables* describing the phase boundaries, or junctions, between the B- and the S-state domains. However, the Ising description can also be interpreted such that in S-state the separation between nearest bases along the chain is increased such that on average the chain has elongated by a factor of $1.7$. This would allow still another denaturation transition to take place for higher forces shown by experiments [30].

### 3.2.1 Two-state Model

To define the two-state model more precisely, we divide the DNA chain into a sequence of short segments of length $a_0$ such that every segment can be said to be either in the B or S state, $\sigma_i$. The state of a "B segment" is denoted by spin up ($\uparrow$) and $\sigma_i = +1$, while that of a "S segment" by spin down ($\downarrow$) and $\sigma_i = -1$. The easiest possible description of this kind of system is provided by a nearest neighbor one-dimensional Ising model, in which the energy spectrum takes on four different values: $\Delta E(\uparrow\uparrow)$, $\Delta E(\uparrow\downarrow)$, $\Delta E(\downarrow\uparrow)$, $\Delta E(\downarrow\downarrow)$, depending on the state of two neighboring segments. Assuming a symmetric spectrum around the middle level $\Delta E(\uparrow\downarrow) = \Delta E(\downarrow\uparrow)$, this spectrum can be parametrized by two quantities $J$ and $H$ as

$$\Delta E(\uparrow\uparrow) = 2H + 4J \tag{3.7}$$

$$\Delta E(\uparrow\downarrow) = \Delta E(\downarrow\uparrow) = 2H \tag{3.8}$$

$$\Delta E(\downarrow\downarrow) = 2H - 4J. \tag{3.9}$$

The Hamiltonian for this kind of nearest neighbor Ising model can be written as

$$\mathcal{H}_{\text{int}} = -J \sum_{i=1}^{N} \sigma_i \sigma_{i+1} - H \sum_{i=1}^{N} \sigma_i. \tag{3.10}$$

The quantities $H$ and $J$ describing the internal degrees of freedom of DNA must be determined either by molecular modeling or by taking them as fitting parameters to be determined by comparison with experiments. Physically, $2H$ can be identified as the zero-tension free-energy difference per segment between the B and S states. The parameter $J$ measures the correlation energy between adjacent segments, and by analogy to the Ising model we can interpret $\exp(-4J/k_{\text{B}}T)$ as a measure of the degree of cooperativity.

Ahsan et al. proposed later a *two-state Worm Like Chain (WLC)*, which is a combination of the two-state model and the elasticity theory of the semiflexible chain free-energy given by Eq. (3.6) in the case $\lambda = \infty$ [1, 18]. Ahsan's idea was to include an additional parameter $\delta$ into this model, describing the fractional elongation of the S state over the B state.

Though one assumes here that the elastic bending energies of S and B states are identical, we will show later that relaxing this constraint makes it possible to include the description of force-induced melting transition into the picture. Finally, the global coupling between the internal structure and chain conformation is provided by the constraint:

$$L(\{\sigma_i\}) = L_0 \left(1 - \frac{\delta}{2N} \sum_{i=1}^{N} (\sigma_i - 1)\right), \tag{3.11}$$

with $L_0$ being the length of the chain in the pure B phase, $N \gg 1$ the number of the segments and $a_0 = L_0/N$ the structural segment length. Thus we see that the chain length $L$ has become a statistical variable whose expectation value has to be determined over the canonical distribution of energy states. From Eqs. (3.10) and (3.6) we can write the total effective Hamiltonian as $\mathcal{H}_{\text{eff}} = \mathcal{H}_{\text{int}} + Lg(f)$. By using this simple description of the tension-induced B-to-S conversion, it is possible to analytically obtain a new force-extension relationship. The derivation was first made by Ahsan et al. [1], and the details are given in Appendix A in article III. Furthermore, the equation of state $y(f) = x/L$ as derived by Ahsan et al. is given by Eq. (3.4) using the bare values of elastic parameters. Ahsan et al. [1] applied this model in the case of zero stretching modulus over the force-extension data by Cluzel et al. [10], and found good agreement with that. Thus, we tried to use the same theory, but instead of the bare elastic moduli, we use the salt renormalized elastic moduli according to Eq. (3.5). Then we tried to fit the present description to the experimental data of Wenner and Williams [70] for different salt concentrations. We used the same values for the Ising parameters $H = 1.75$ and $J = 1.25$, and for the elongation parameter $\delta = 0.78$, as Ahsan et al. [1]. The segment length of DNA was taken to be $a_0 = 0.34$ nm corresponding to one base pair. By plotting the resulting theoretical curves against experimental results, we found that this kind of *description does not reproduce the change in the overstretching force* according to the experiments of Wenner and Williams [70], as the salt concentration is varied.

### 3.2.2 Change of Elastic Moduli During the Overstretching Transition

One can speculate that the approach above failed because the elastic energies of B and S segments were treated as equal. This idea is supported by experiments. It has been shown that the force required to stretch the chain rises again after the plateau in the force-extension curve, with a slope that depends on pulling rate. The rise continues up to about 140 pN, where the $f$–$x$ curve of double-stranded DNA (dsDNA) then matches that of single-stranded DNA (ssDNA) [9]. As we pointed out in Sec. (3.1), the elastic moduli of ssDNA differ significantly from those of dsDNA [68]. Thus, one is tempted to conclude that models where elastic parameters along DNA are treated as constants are not adequate. Rather, it would be justified to aim for a full description of the force-extension curve through a model in which the elastic parameters are allowed to change along DNA over the transition.

As an improvement to the model described in Sec. (3.2.1), we proposed a model where an internal structural state of the DNA molecule is described by segments in the B-state, or double-stranded state, and segments in the S-state, or the denatured state. We model the segments in the S-state as two slightly separated, but parallel strands still coupled together electrostatically, in the sense that they interact electrostatically in a way similar to segments in the B-state. In other words, we do not make distinction between an over-stretched DNA molecule and one that is fully in the denatured state. This assumption is consistent with the experimental finding [9, 70] that the behavior of a DNA molecule stretched beyond the overstretching plateau is close to that of a ssDNA molecule.

We then construct the following ansatz for the effective free energy associated with an internal structural state of a WLC under a constant force:

$$H_{\mathrm{WLC}} = \frac{L}{N} \sum_{i=1}^{N} \left[ \delta_{\sigma_i,+1}\, g_{\mathrm{ds}}(f) + \delta_{\sigma_i,-1}\, g_{\mathrm{ss}}(f) \right], \tag{3.12}$$

where Kronecker symbols $\delta_{\sigma_i,\pm 1}$ have their usual mathematical meaning. Here $g_{\mathrm{ds}}(f)$ and $g_{\mathrm{ss}}(f)$ are free-energy densities corresponding to a pure B-state (double-stranded state)

and a pure S-state (denatured state) DNA molecule, respectively. They have the same functional dependence on the applied force $f$ as that described in Eq. (3.6), but involve different renormalized elastic moduli, corresponding to the B-state and the S-state DNA, respectively.

Our model ansatz provides a simple, minimal remedy for the limitation of the linear-combination model description of the elastic properties. This point can be made clear if we re-express the total free energy – the sum of Eq. (3.10) and Eq. (3.12) – associated with an internal state in terms of the internal state variables, $\sigma_i$'s. With very little algebra, we arrive at the following explicit form:

$$\begin{aligned}\mathcal{H}_{\text{eff}} = & - J \sum_{i=1}^{N} \sigma_i \sigma_{i+1} - \tilde{H}(f) \sum_{i=1}^{N} \sigma_i \\ & - \frac{L_0 \delta}{4N^2} [g_{\text{ds}}(f) - g_{\text{ss}}(f)] \left( \sum_{i=1}^{N} \sigma_i \right)^2 + \frac{L_0}{2} (1 + \frac{\delta}{2}) [g_{\text{ds}}(f) + g_{\text{ss}}(f)],\end{aligned} \tag{3.13}$$

where the effective external field $\tilde{H}(f)$ is given by $\tilde{H}(f) = H - \frac{a_0}{2}[g_{\text{ds}}(f) - (1+\delta) g_{\text{ss}}(f)]$. It is easy to see that the second line in Eq. (3.13) indeed describes a global, or infinite range, coupling between the internal state variables $\sigma_i$'s.

We can try to justify the form of our ansatz as follows. First, it assigns the WLC free energy the property of extensivity as a function of $L$. Second, it reduces to the two right limiting cases corresponding to the B- and the S-state. Third, within the framework of Ising model, the ansatz in Eq. (3.13) is the simplest possible long-range coupling between the B-state and the S-state. The strongest argument, however, is the physically meaningful fitting to the experimental data, which is explained in Sec. 3.3.

As a word of warning, our ansatz Eq. (3.12) treats each segment of length $L/N$ as if it were a semiflexible polymer described by stretching and bending moduli. In the case of DNA, the segment length is equal to $a_0 = 3.4$Å, which is very short. As a remedy, we have noticed that if the coherence length for both B-state and S-state segments is longer than the persistence length in each state, respectively, the ansatz used is meaningful. We

have checked that for the parameters we consider this is in fact the case.

Given the effective "Hamiltonian" associated with a single internal structural state of the DNA molecule, Eq. (3.13), we performed the statistical ensemble average over all possible internal states and evaluated the partition function and calculated the force-extension relation, shown in Appendix 1 of Article III. Using the final interpolation formula for the force-extension curve Eq. (21) in Article III, we may now compare our theory with experimental data.

## 3.3 Comparison with Experiments

In principle, the fitting involves two effective charge separations, one for the B- and one for the S-state. It turns out that numerically only one of them can be fitted accurately, namely the charge separation $c$ in the S-state. This means that the two chains are electrostatically coupled such that the effective charge separation is determined by the *overstretched strands* of DNA. The salt dependence of the fitting parameters $J$, $H$, $c$, and $\delta$ are determined by a nonlinear least-squares fitting method using all the data measured by Wenner and Williams [70]. This set of experimental data was chosen for comparison because, to our knowledge, it is the most comprehensive one in terms of the salt dependence of the overstretching transition.

In the fitting procedure, the bare elastic moduli are given in the B-state by Wenner et al. in 1 M case [70], i.e. $\lambda_{\rm ds} = 1256\,$pN and $K_{\rm ds}/k_{\rm B}T = 46\,$nm. In the single-stranded state we fixed the bare values of elastic moduli to be such that our theoretical force-extension curve interpolates between the experimental results for dsDNA and the ssDNA $f$–$x$ curve to minimize the error [9]. These bare values are given by $\lambda_{\rm ss} = 920\,$pN and $K_{\rm ss}/k_{\rm B}T = 0.75\,$nm. Later, the salt dependence of elastic moduli in both ds- and ss-state are given by Eq. (3.5). The salt dependence of the remaining adjustable Ising structural and electrostatic parameters are adjusted close to the overstretching plateau in an almost

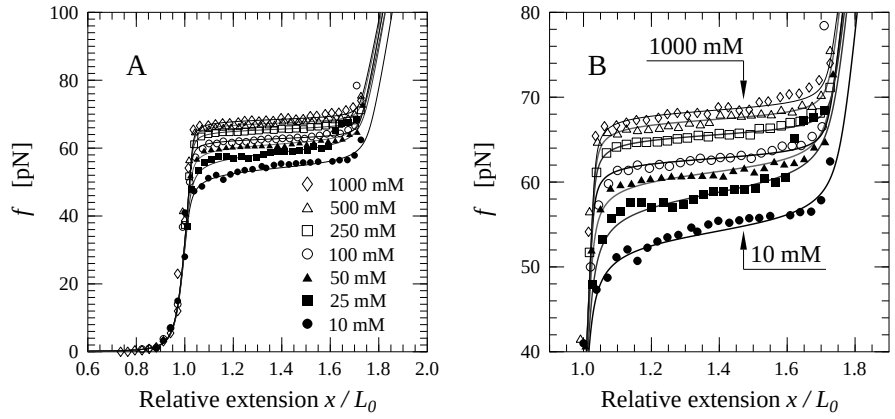


**Figure 3.1**: Room temperature force-extension curves for a single dsDNA molecule in different salt concentrations. The solid lines correspond to theoretical curves calculated using the global coupling theory developed in this work. Experimental data is by Wenner et al. [70]. A) Data over all regimes showing the complete force-extension curves. B) The same data showing only the overstretching portion.

unique fashion. Overall, we found that it was not possible to prepare two equally good fits with different sets of values for the structural and electrostatic parameters.

The parameter values corresponding to the optimal fitting are given in Table 1 of Article III. Based on these values, as depicted in Fig. 3.1, the theoretical model developed here describes the experimental data of Wenner et al. notably well for all salt concentrations.

Having found that the present theory describes experimental data very well, let us discuss the conclusions we can draw based on this work. The main conclusion of the numerical study is that the whole force-extension curve can be fitted to numerical data only if the salt dependence of the effective charge separation $c$ is taken into account. All the other parameters remained by and large constant, as can be seen from Table 1 of Article III. Importantly, we further find that $c$ interpolates between the structural length $a_0$ of 0.17 nm at high salt (no effect of electrostatics) and the Bjerrum length $l_{\mathrm{B}}$ of 0.74 nm in water in the no-salt limit (strong electrostatic coupling). These results are consistent with Manning and Poisson-Boltzmann theories for thin polyelectrolyte rods [4, 42]. In that case, it is

shown that if the linear charge density $\tilde{R} = q_c l_B/c$ exceeds the critical value 1, then the fraction $1 - 1/\tilde{R}$ of counterions condenses onto polyelectrolyte. Here the counterion valency $q_c = 1$, since we are considering DNA in 1:1 electrolyte. The problem is how to determine $c([\mathrm{Na}^+])$. In the limit of infinite salt, however, all the electrostatic effects are washed away, and the renormalized distance between the charges along polyelectrolyte is just the structural length $a_0$. On the other hand, in the $\kappa \to 0$ limit all the counterions are condensed, and the distance between a unit charge along the polyelectrolyte close to it is equal to the Bjerrum length. We discuss the significance of these findings below.

The first question about the validity of our ansatz Eq. (3.12) concerns the non-linear effects of electrostatics in the low salt regime into the overstretching transition. For low salt concentrations, the interaction strength parameter $J$ varies slightly, see Table 1 in Article III. This is mainly due to the fact that the elasticity theory of Podgornik et al. breaks down in the zero-salt limit [56], but also partly due to lack of long-range interactions in the Ising model description of hydrogen bonds. In other words, the approximations used in Eq. (3.12) may break down, if the (electrostatic) interaction is strong enough (low salt), or if the Hamiltonian includes many-body effects not taken into account by the Ising model. The latter is true, in fact, for the so-called base-stacking of DNA, and may give a significant contribution to the total interaction energy [2].

To characterize the cooperativity of the B-to-S transition, we used a similar analysis as introduced already by Rouzina and Bloomfield [63]. In order to justify our free energy ansatz Eq. (3.12), we have to guarantee that the average sizes of both B- and S-clusters are larger or of the order of the persistence length. By using the formulas given in Ref. [63] we found that the average number of base pairs in both type of clusters is roughly 30. For the S-DNA this is clearly larger than its persistence length 1.5bp. However, for B-DNA 30 correlated base pairs is smaller than its persistence length of about 150bp. However, the number of base pairs changes very rapidly with force, meaning that already at the turning points of the plateau, the number of base pairs exceeds the critical value 150, being $k_{ss} = k_{ds} \approx 180$ bp at 1M of salt, and $k_{ss} = k_{ds} \approx 300$ bp, for 10mM case.

We also studied the dependence of the overstretching transition on the salt concentration. As we can see from Fig. 3.1, the increase in the overstretching force is correctly reproduced by our final force-extension curve. This seems to rule out the need for any logarithmic corrections in the free energy to explain the change in reference state used by other groups [63, 64, 70]. In fact, by expanding the renormalized stretching parameter $\lambda^R$ around $\kappa b \ll 1$, one can see that the overstretching force depends logarithmically on $\kappa b$. To better understand the changes that take place during DNA overstretching, we can use our analytical results to predict the explicit [$Na^+$] dependence of the overstretching force. A good estimate of the overstretching force may be given by the force value, at which the renormalized external field $\tilde{H}$ changes sign from positive to negative. Mathematically, this is defined by the following equation:

$$\tilde{H}(f) = H - \frac{a_0}{2}[g_{\rm ds}(f) - (1+\delta)g_{\rm ss}(f)] = 0. \tag{3.14}$$

Thus, for all values of the salt concentration we have an estimate for the overstretching force. Clearly, for low ionic strengths this equation agrees with the logarithmic form given by Wenner et al. [70]. In the regime of high salt concentrations, our model achieves more than that used by Wenner et al. [70], and can be linearized to give the leading order salt dependence as

$$f_{\rm ov} = f^0_{\rm ov} + \Delta f_{\rm ov} \simeq 81.7\,{\rm pN} - \frac{4.29}{(\kappa a)^2}\,{\rm pN} - 0.477\,h(\kappa b)\,{\rm pN}, \tag{3.15}$$

where $b$ is the microscopic cutoff, often assumed to be of the order of the thickness of DNA, i.e. 1nm, and $h(x)$ is defined by $h(x) = {\rm e}^x - {\rm Ei}(-x)$. Equation (3.15) provides a reasonably good approximation for the overstretching force with salt concentrations higher than 100 mM. In addition, one can notice that the logarithmic dependence of overstretching force on $\kappa b$ comes out automatically in the limit $\kappa b \ll 1$.

## 3.4 Conclusions

Article III deals with the salt dependence of force-induced overstretching transition of DNA, with a focus on two major questions, namely, (i) whether the electrostatic com-

ponent of the B-to-S transition is a manifestation of effects already accounted for in the mesoscopic elasticity, or whether other (local or global) effects are involved, and (ii) how well the data analyzed conform to the much invoked Manning condensation theory [42].

To address these questions theoretically, we have developed a model which combines the Ising model description of internal structure used by Ahsan et al. [1] and the elasticity theory by Podgornik et al. [22, 56]. Furthermore, we have extended the model to account for effects of electrostatics (salt) on structural and Ising parameters, by fitting our force-extension relation to experimental data.

Based on the theoretical model, we have predicted the force–extension relation (or curve) as a function of the relevant parameters, which in turn depend on the salt concentration. We have then fitted the theoretical prediction with the available experimental data, and from the fitting determined the numerical values of the model parameters as functions of the salt concentrations.

The main conclusion of the study are:

(a) One has to include the change of bare elastic moduli for each segment during the overstretching transition into theory, in order to get successful fitting. A minimal model to describe this effect is given by Eq. (3.12).

(b) The fitting between the theoretical prediction and the experimental data works remarkably well for all of the salt concentrations investigated. Moreover, the fitting reveals that the parameter that is most sensitive to the salt concentration is the effective length of charge separation. As shown in Table 1 of Article III, the salt-dependence of the effective charge separation *varies consistently with Poisson-Boltzmann and Manning condensation theories for thin rods*, i.e., from about 0.67 nm at low 1 mM (monovalent) salt, to 0.17 nm at 1000 mM salt. These results show that the fit between our model prediction and the experimental data

is not only of good numerical quality, but is also physically meaningful.

(c) Within the range of validity of the theory, corresponding roughly to salt concentrations exceeding physiological salt concentrations (100 mM for monovalent salt), the Ising structural constants $J$ and $H$ have no salt dependent electrostatic components.

Based on these results, we may draw the conclusion that our model is successful in interpreting the experimental overstretching data, despite of its crudeness. The good fit between our theory and the experimental data suggests that this simple effective approach may have captured in a nontrivial way the most essential aspects of the complex electrostatic interactions.

The only thing our theory does not predict explicitly is the salt-dependence of the effective separation between unit charges along the DNA $c([\mathrm{Na}^+])$. Basically, this could be obtained by first solving the counterion distribution around the chain like in Sec. 2, and then integrating the amount of bound counterions on the surface of the chain. To include this effect into the model, one has to use a SC-model for electrostatic interaction energy to account for nonlinearities. Anyhow, the theoretical framework of Manning condensation works beautifully in the limit of large salt concentration, where the nonlinearities are less significant. Thus, our hybrid theory works very well for salt concentrations exceeding the physiological salt concentration 100 mM.

# 4 Scaling Analysis for the Sedimentation of Polymer

In the previous Sections we have been developing tools how to describe the electrostatic, elastic and internal degrees of freedom of the DNA molecule. However, the dynamical aspects have not been of interest yet, since we have only considered the equilibrium distribution of ions around DNA, and equilibrium shape of DNA under traction.

Here we want to study the sedimentation of a semiflexible interacting polymer chain, such as the DNA, but in the presence of a large concentration of salt, such that the role of electrostatic repulsion between the monomers is mainly to prevent the monomers of collapsing onto each other. In other words, we consider a chain of monomers interacting through the excluded volume interaction, where the role of electrostatic repulsion is to increase the excluded volume compared to the absence of electrostatics, and to renormalize the elastic moduli, as in Sec. 3. Also, we consider the properties of a polymer chain in the largest scales, where the biggest contribution to the elastic energy becomes from the stretching of the chain, i.e., $\mathcal{H}_e \propto \frac{1}{2}\lambda \dot{\mathbf{r}}(s)^2$.

The sedimentation of DNA has become very interesting lately, due to the development of the ultracentrifugation techniques for separation and characterization of biomolecules like proteins [24]. Here the most interesting aspect is to find out the relationship between the conformation of the sedimenting biomolecules and its limiting sedimentation velocity $\mathbf{v}_{lim}$, since the separation between the components of the sample depends only on the limiting velocity of the molecule. It has been shown both experimentally [7, 65] and theoretically [76] that for a long DNA in dilute solution, the sedimentation velocity decreases by increasing the rotor speed. This is a consequence of the hydrodynamic shielding of the interior of DNA, which causes the drag reduction for the core part compared to the coil exterior. Thus, the chain ends that are located at the coil exterior, lag behind due to

increased friction, and the chain extends. Later, it has been shown through hydrodynamic simulations [66] that in the limit of zero Reynolds number the polymer chain consists of a compact leading part and a stretched trailing part. This picture seems to be consistent with experiments, though these simulations neglect the effect of inertial forces.

The sedimentation of rigid bodies such as spheres and spheroids and rods is well understood in dilute limit. However, at finite volume fractions even the dynamics of simple spheres is highly nonlinear. While considering a polymer chain, one has a many-body object with complicated elastic and internal interactions that we considered in Sec. 3. Thus it is easy to believe that the dynamics of a sedimenting polymer contains very rich physics at different length and time scales.

In studying the dynamics of polymers generally, there are two key quantities one should pay special attention for. The first is the radius of gyration, a measure of the volume the polymer occupies. It is defined as

$$R_G \equiv \sqrt{\frac{1}{N}\sum_{i=1}^{N}\langle(\mathbf{r}_i - \mathbf{R}_{CM})^2\rangle}, \tag{4.1}$$

where $N$ is the number of monomers, $\{\mathbf{r}_i\}$ are the positions of the monomers, and $\mathbf{R}_{CM}$ is the center of mass (CM) of the polymer, i.e. $\mathbf{R}_{CM} = \frac{1}{N}\sum_{i=1}^{N}\mathbf{r}_i$. This is a purely static quantity, but it is also the most interesting one, since it characterizes the size of the polymer.

The second important quantity is the CM diffusion coefficient

$$D_{CM} \equiv \lim_{T\to\infty}\int_0^T \mathrm{d}t\langle\delta\mathbf{v}_{CM}(t)\cdot\delta\mathbf{v}_{CM}(0)\rangle \tag{4.2}$$

and it is more interesting from the dynamics point of view, since it describes how small fluctuations in the velocity of the CM of the polymer decay as a function of time.

In the symmetric problem the radius of gyration and the CM diffusion coefficient scale as a function of the monomers as $R_G \propto N^{\nu}$ and diffusion coefficient as $D \propto N^{\nu_D}$, where $\nu$

and $\nu_D$ are *universal* scaling exponents.

However, in the case of a sedimenting polymer chain, there exists a symmetry breaking force field, namely the gravitational force. Clearly, it pushes all the monomers in the direction of sedimentation that we will call the parallel direction. This has dramatical consequences, since it changes the shape of the polymer such that the traditional scaling does not hold anymore, but instead the polymer deforms slightly in the direction of sedimentation. The polymer chain has two characteristic sizes, in the parallel direction to sedimentation $R_{G,\parallel}$, and in the direction perpendicular to sedimentation $R_{G,\perp}$, so that the scaling law should transform into

$$\begin{aligned} R_\perp &\propto N^{-\nu_\perp}; \\ R_\parallel &\propto N^{-\nu_\parallel}. \end{aligned} \tag{4.3}$$

As a consequence, also the scaling of diffusion coefficient separates into two components:

$$\begin{aligned} D_\perp &\propto N^{-\nu_{D,\perp}}; \\ D_\perp &\propto N^{-\nu_{D,\perp}}. \end{aligned} \tag{4.4}$$

The very intriguing problem here is to develop a theory to describe the dynamics of a polymer under the gravitational force, and to predict the scaling exponents and their dependence on the limiting velocity and the Reynolds number.

In Article IV we model quantitatively the steady-state sedimentation of a single polymer chain in a good solvent. Here, we explain partly those findings, but we also show new theoretical results obtained more recently [58]. We study the scaling of the radius of gyration and the velocity fluctuations under steady state, by using analytical derivations for the velocity field around the falling polymer, and the probability distribution function of the chain. Based on these considerations, we propose scaling arguments for both components of radius of gyration, and for the chain diffusion coefficient as well, that are in good harmony with our numerical findings.

## 4.1 Model

The model system we simulated in this work is described in Section 3.3 of Article IV of this Thesis. Basically it contains a continuum description for the solvent that is modeled using the incompressible Navier-Stokes (NS) equation, coupled through no-slip boundary conditions to the polymer molecule. Polymer is described using the standard bead-spring model, with a repulsive Lennard-Jones type pair potential between all beads to prevent overlapping, presenting excluded volume interactions, and a spring type FENE potential between adjacent segments, describing the stretching energy. In this model, there are no thermal fluctuations, meaning that the particles are non-Brownian, with an effective temperature of $T = 0$, or infinite Péclet number. Consequently, this means that entropy does not play any role here, while considering the equilibrium configurations of the polymer.

To develop a theoretical model for this kind of a system, one needs to consider the NS equations coupled to the motion of beads or monomers of the polymer. In mathematical terms the NS-equations read as

$$\rho(\partial_t \mathbf{v} + \mathbf{v} \cdot \nabla \mathbf{v}) = -\nabla P + \eta \nabla^2 \mathbf{v} + \mathbf{f}, \tag{4.5}$$

together with the incompressibility condition $\nabla \cdot \mathbf{v} = 0$. Eq. (4.5) can also be written in a dimensionless form such that the only parameter that is left is the Reynolds number, defined as

$$Re = \frac{\rho U L}{\eta}, \tag{4.6}$$

where $U$ and $L$ are typical velocity and length scales of the problem, respectively, $\eta$ is the bulk viscosity and $\rho$ the density of the fluid.

In the case of an asymmetric polymer chain, one actually has two characteristic Reynolds numbers; one for the direction of the gravity, and one perpendicular to it, characterized by $R_{\parallel}$ and $R_{\perp}$, respectively. The characteristic velocity field is naturally the settling speed of the chain.

In the level of linearized hydrodynamics, the velocity of each monomer $n$ is assumed to be given by the Oseen tensor [59]

$$\mathbf{v}_n = \sum_m \mathbf{H}(\mathbf{r}_n - \mathbf{r}_m) \cdot (-\nabla_n U(\{\mathbf{r}_n\})) \,, \tag{4.7}$$

where $\mathbf{H}(\mathbf{r} - \mathbf{r}')$ is the Green's function of Eq. (4.5), in the case $Re = 0$. This allows one to write the velocity field more generally at an arbitrary point in space as a linear combination of forces acting on it

$$\mathbf{v}(\mathbf{r}) = \sum_{n=1}^{N} \int \mathrm{d}\mathbf{r}' \mathbf{H}(\mathbf{r} - \mathbf{r}_n) \cdot \mathbf{f}_n. \tag{4.8}$$

However, in this study we were not interested in the $Re = 0$ limit, but actually we wanted to consider the effect of a non-zero Reynolds number on the conformation of the sedimenting polymer chain. The focus is on finding the steady-state equilibrium averages for radius of gyration and diffusion coefficient. The problem is that in the simulations of Article IV $T = 0$, and one basically does not have a canonical distribution with respect to temperature. However, in the problem of sedimenting polymer the configuration of the polymer chain is changing continuously, inducing also continuous velocity fluctuations into NS fluid. Thus we can define an effective temperature using Green-Kubo theory [21] as

$$k_B T_{eff} = \frac{1}{V\eta} \int \mathrm{d}t \langle \Pi_0^{\alpha,\beta}(t) \Pi_0^{\alpha,\beta}(0) \rangle, \tag{4.9}$$

where $V$ is the volume of the system, and $\Pi_0^{\alpha,\beta}$ is the off-diagonal element of the Fourier transformed viscous stress tensor in the limit $\mathbf{k} \to 0$. In real space the viscous stress tensor is defined as

$$\Pi^{\alpha,\beta}(\mathbf{r}, t) = \delta_{\alpha,\beta} P(\mathbf{r}, t) - \eta \left( \frac{\partial v_\alpha(\mathbf{r}, t)}{\partial r_\beta} + \frac{\partial v_\beta(\mathbf{r}, t)}{\partial r_\alpha} \right) + \frac{2}{3} \eta \delta_{\alpha,\beta} \nabla \cdot \mathbf{v}(\mathbf{r}, t) \tag{4.10}$$

where $\{P(\mathbf{r}, t), )\mathbf{v}(\mathbf{r}, t)\}$ is the solution to Eq.(4.5).

Assuming close-to-equilibrium conditions gives us an effective way to calculate canonical averages of monomer coordinates and monomer momenta over the distribution function

$$\psi(\mathbf{p}_n, \mathbf{r}_n) = \frac{e^{-\beta_{eff} \sum_n [\frac{\mathbf{p}_n^2}{2m} + U(\{\mathbf{r}_n\})]}}{\mathcal{Z}}, \tag{4.11}$$

where $\mathcal{Z}$ is the canonical partition function for the system, defined as

$$\mathcal{Z} = \prod_{n=1}^{N} \int \mathrm{d}\mathbf{p}_n \mathrm{d}\mathbf{r}_n e^{-\beta_{eff} \sum_n [\frac{\mathbf{p}_n^2}{2m} + U(\{\mathbf{r}_n\})]}, \tag{4.12}$$

and $\beta \equiv (k_B T_{eff})^{-1}$. Typically one integrates the canonical momenta, but here we argue that it cannot be done in our case, since $\beta_{eff}$ and $\delta \mathbf{v}_{CM}$ are related to each other, and are both functions of the radius of gyration of the polymer chain. Our strategy is to solve the velocity field from the NS equation (4.5), and obtain an effective kinetic energy that depends only on the monomer coordinates.

## 4.2 Results

Here we present our numerical and theoretical results for the radius of gyration and the diffusion coefficient of the sedimenting polymer chain. The main achievements are explicit expressions for the scaling exponents of radius of gyration and diffusion coefficient in both directions, parallel and perpendicular to the gravitational field. These are given in Secs. 4.2.2 and 4.2.3.

### 4.2.1 Radius of Gyration

Starting from an initial state with zero velocity, it takes the polymer chain typically less than about 1500 single particle Stokes times to reach its steady state distribution. In the steady state, we determined the components of average radius of gyration from Eq.(4.3). Without loss of generality, we have chosen the coordinate system such that the gravitational force points towards the negative $z$ axis. Thus, $z$ axis is the direction parallel to the flow ($\|$), and the $xy$ plane is perpendicular ($\perp$) to it. In Fig. 4.1 we show a time series of behavior of the two components of the radius of gyration for $N = 32$. The steady-state is characterized by large fluctuations in the size of the polymer, and the overall radius

of gyration is larger perpendicular to the flow for this value of $N$. It is interesting to notice that the polymer seems to have two characteristic shapes, where the polymer is either extended along the flow (with large $R_{G,\parallel}$) or in the plane perpendicular to it (large $R_{G,\perp}$). Furthermore, the extended configuration relaxes quickly back to the $xy$ plane, but the motion in the plane perpendicular to $z$ happens much more slowly. The minima and maxima for these two components of $R_G$ are temporally out-of-phase, as expected. These observations are in accord with the experimental and numerical results which have indicated that rods and spheroids happen to align themselves perpendicular to the gravitational field, when the Reynolds number is non-zero [33]. This is the total opposite to the case of vanishing Reynolds number $Re = 0$, where these objects keep their initial conformation, which is due to time reversability of the Stokes equation.

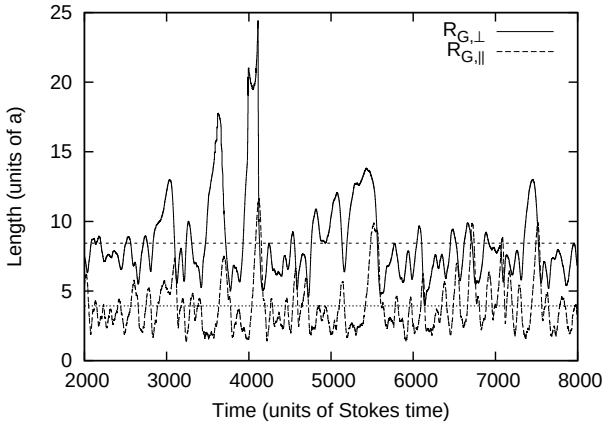


**Figure 4.1**: Raw data for the components of the radius of gyration with $N = 32$ in the steady-state. The vertical lines indicate the average value of the respective component, calculated from the whole simulation data, of which only a small part is shown in the figure.

In Fig. 4.2 we show snapshots of typical configurations corresponding to two different conformations. We also show how the transition occurs between these two different conformations. First, self-avoidance extends the polymer in the direction perpendicular to gravity. Then, the end of the chain lacks behind due to the higher friction in the exterior of the polymer coil. As a consequence, the polymer *tail* is elongated in the positive $z$ direction, to a rod-like configuration, which quickly relaxes back onto the $xy$ plane. The tail

part is pulled down by the gravitational force caused by the head part, due to difference in the friction felt by these two parts of the polymer. Finally, the self-avoiding effects extend the relaxed chain in the perpendicular direction, and the polymer returns back to its original horizontally extended state.

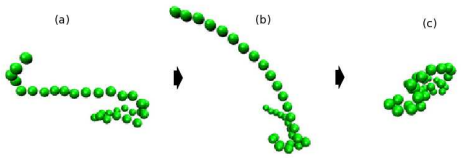


**Figure 4.2**: (Color online) Snapshots of typical configurations of a settling polymer with $N = 32$ in the steady-state. The polymer is elongated in the horizontal direction (a). The loose end of the polymer feels higher friction, and the polymer end lacks the head part of the chain in the vertical direction (b). The gravitational force of the head part pulls the part that is left behind, and the polymer collapses into a globular shape (c), which then expands due to self-avoidance leading back to a shape of the type in (a).

We also noticed that the time series data indicate a perfect correlation between the polymer's CM velocity and $R_{G,\perp}(t)$. This is in qualitative agreement with the Stokes friction formula that the limiting velocity should be inversely proportional to the component perpendicular to flow of the radius of the object, namely $v_{\|} \propto \mathbf{F}/R_{G,\perp}$, where $\mathbf{F}$ is the gravitational force acting on the CM of the polymer, i.e. $\mathbf{F} = Nmg\mathbf{e}_{\|}$. We will use this result in Sec. (4.2.2) to justify the velocity decomposition.

In Fig. 4.3 we show the actual distributions for $R_{G,\|}$ and $R_{G,\perp}$ for chains of length $N = 16$, $28$ and $32$. These distributions are quantitatively different from the usual distribution of $R_G$ in equilibrium. The spatial symmetry-breaking induced by gravity is also clearly seen.

In Article 4 of this Thesis we found that power-law scaling for both components of radius of gyration is well satisfied, and gives $\nu_{\|} = 0.79 \pm 0.02$ and $\nu_{\perp} = 0.45 \pm 0.01$. For comparison, we also calculated the scaling of the total radius of gyration $R_G \sim N^{\nu}$, with $\nu = 0.50 \pm 0.01$, indicating that the perpendicular component of radius of gyration

determines the size of the polymer, for the recent parameter values. All these values are clearly different from the 3D self-avoiding walk exponent in equilibrium, which is $\nu_e = 0.588$ [12]. The larger scaling exponent of the parallel component indicates that the ratio $R_{G,\parallel}/R_{G,\perp}$ actually *grows* with increasing $N$, and thus the parallel component becomes eventually larger than the perpendicular one for long enough chains assuming that the present scaling holds for larger values of $N$ as well. This result can be interpreted as follows; the tail-head structure of the polymer becomes the more pronounced the longer the chain is. Then finally, at some critical value of $N$, the friction of the elongated polymer finally decreases below the friction felt by the head of the polymer, after which the chain is fully elongated. We suppose the small head regime still stays for infinitely long chains as well. These numerical findings are in qualitative agreement with a recent numerical study of polymer sedimentation with $\mathrm{Re} = 0$ [66].

### 4.2.2 Generalized Flory Argument

For a polymer chain in thermal equilibrium, the classic Flory mean-field argument [12] gives a very good approximation of the true scaling exponent for $R_G(N)$. In order to explain the numerical scaling results in the previous section, we present here a generalization of the Flory argument for the present case of a polymer chain in a steady-state flow. We assume that the equilibrium distribution function is given by Eq. (4.11), and then we further calculate the polymer distribution function as a function of the end-to-end

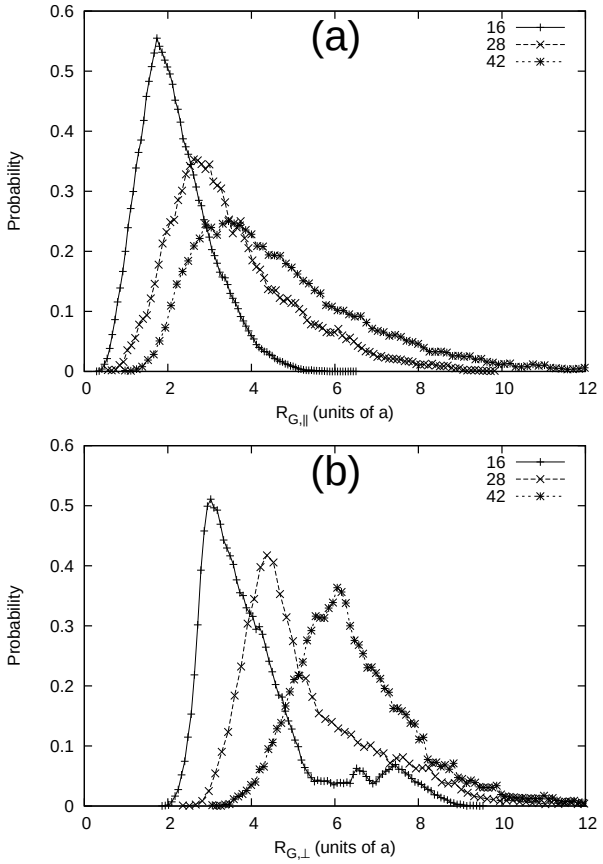


**Figure 4.3**: The distributions of the two components of the radius of gyration: (a) in the direction parallel to gravity, and (b) in the direction perpendicular to gravity. The chain lengths are indicated in the figures.

distance and the CM momenta [12] as

$$\begin{aligned}
\Psi(\mathbf{R},\mathbf{P}) &= \prod_n \int \mathrm{d}\mathbf{r}_n \int \mathrm{d}\mathbf{p}_n \psi(\{\mathbf{r}_n\},\{\mathbf{p}_n\})\delta(\mathbf{R}-\sum_n[\mathbf{r}_n-\mathbf{r}_{n-1}])\delta(\mathbf{P}-\sum_n \mathbf{p}_n) \\
&\equiv \langle e^{-\beta_{eff}[U(\{\mathbf{r}_n\})+E_K(\{\mathbf{p}_n\})]}\delta(\mathbf{R}-\sum_n[\mathbf{r}_n-\mathbf{r}_{n-1}])\delta(\mathbf{P}-\sum_n \mathbf{p}_n)\rangle \\
&= \langle e^{-\beta_{eff}[U(\{\mathbf{r}_n\})+\frac{1}{2}\frac{\mathbf{P}^2}{Nm_0}]}\delta(\mathbf{R}-\sum_n[\mathbf{r}_n-\mathbf{r}_{n-1}])\rangle \\
&\geq e^{-\beta_{eff}\langle\left[U(\{\mathbf{r}_n\})+\frac{1}{2}\frac{\mathbf{P}^2}{Nm_0}\right]\rangle} \\
&\equiv e^{-\beta_{eff}\left[U(\mathbf{R})+\frac{1}{2}\frac{\mathbf{P}^2}{Nm_0}\right]},
\end{aligned} \tag{4.13}$$

where the inequality follows from the variational principle of Feynman [14]. Later, the CM momentum $\mathbf{P}$ is to be calculated in what follows from the NS equation. It will be shown that it depends only on the polymer radius of gyration $R_{\|}$. Thus, the total free energy of the polymer chain consists of the spring forces between the monomers, the self-avoidance and the kinetic energy contribution, and can be written as

$$\begin{aligned}\mathcal{F}_{total} &= -\frac{1}{\beta_{eff}} \log \Psi(\mathbf{P}, \mathbf{R}) \\ &\leq E_{harmonic} + E_{SAW} + E_{kinetic} \\ &\leq \frac{1}{2}\frac{k}{N} R_G^2 + \frac{1}{2}\nu c^2 R_G^3 + \frac{1}{2}(m_0 N)\mathbf{v}_{\mathrm{cm}}(R_G)^2,\end{aligned} \tag{4.14}$$

where $N$ is the number of monomers, $k$ is the spring constant between two monomers, $m_0$ is the mass of one monomer, and $c \simeq N/R_G^3$ is the concentration of monomers per volume. Furthermore, $\mathbf{v}_{\mathrm{cm}}(R_G) = \mathbf{P}/Nm_0$ is the velocity of the center of mass for a given radius of gyration $R_G$. The kinetic term describes non-equilibrium behavior, and setting it to zero recovers the equilibrium scaling limit of Flory [15]. If we assume that the velocity field adapts infinitely fast to configurational changes of the chain, we can say that $\mathbf{v}_{cm} \equiv \mathbf{v}_{cm}(R_G)$.

Next we try to calculate the average kinetic energy of the polymer CM. We make a crude approximation that the velocity of the polymer chain reminds that of a sphere. This is based on the observation that on average the polymer stays on the $xy$ plane perpendicular to gravity, and it has a quasi-spherical shape described by $R_{\perp}$. However, the chain ends tend to elongate upwards like in Fig. 4.2, and then they reverse quickly back to the $xy$ plane. This suggests that the average size of these elongated chain ends is $R_{\|}$. Later, we think that the CM velocity can be divided into an average limiting velocity $\mathbf{v}_{lim}$, describing the settling of the head of polymer chain, and a fluctuation part. The fluctuating part describes the average velocity difference between the head of chain and the elongated chain end. These tail fluctuations are caused by the gravitational force of the head part, mediated via the internal friction.

It has been shown that in the limit $Re = 0$, the vertical velocity of a sphere [72]

$$\mathbf{v}_{lim} \rightarrow \frac{Mg}{6\pi\eta R_{G,\perp}}. \tag{4.15}$$

However, here we want to extend Eq. (4.15) to take into account the effects of inertia as well. In Article IV we showed that one can write the connection between the limiting sedimentation velocity and number of monomers as a power-law:

$$v_{lim} \propto N^{\beta-\nu_\perp}, \tag{4.16}$$

where the exponent $\beta$ reduces to $1$ in the limit $Re \rightarrow 0$, and on the other hand $\beta \rightarrow 0.5$ in the limit of large Reynolds number $Re \gg 1$.

To consider velocity fluctuations, we used the following strategy: In the NS-equation Eq. (4.5) we divide the velocity into two parts, the limiting velocity $\mathbf{v}_{lim}$, and the fluctuation part $\delta\mathbf{v}$. The limiting velocity is now just a constant given by Eq. (4.16), and it only couples to the fluctuation part through the convective term of the NS equation, Eq. (4.5).

The fluctuation part describes changes in the velocity field, and is assumed to be caused by the fluctuating tail of polymer chain. Furthermore, the crude approximation here is that velocity fluctuations obey the linearized Navier-Stokes equation as

$$\rho(\frac{\partial\delta\mathbf{v}}{\partial t} + \mathbf{v}_{lim}\cdot\delta\mathbf{v}) = -\nabla P + \eta\nabla^2\delta\mathbf{v} + \mathbf{f}_{int}, \tag{4.17}$$

where we have linearized the non-linear convective part.

The next step is to consider the *velocity of the tail relative to the head* in the fluid generated by falling polymer. The *CM velocity of the tail* is obtained in the limit of $t \rightarrow \infty$ as

$$\begin{aligned}\delta\mathbf{v}_{CM,tail} &= \frac{1}{N_{tail}}\sum_{n=1}^{N_{head}}\mathbf{v}(\mathbf{r}_n) \\ &= \frac{1}{N_{tail}}\sum_{n=1}^{N_{tail}}\sum_{m=1}^{N_{head}}\mathbf{H}(n,m)\cdot\mathbf{f}_m,\end{aligned} \tag{4.18}$$

where $\mathbf{H}(n,m)$ is the pre-averaged Oseen tensor of Eq. (4.17) in the limit $t \to \infty$, and it can be written as [12, 59]:

$$\mathbf{H}(n,m) = \langle \frac{1}{(2\pi)^3} \int \mathrm{d}^3\mathbf{k} \frac{e^{-i\mathbf{k}\cdot(\mathbf{r}_n - \mathbf{r}_m)}}{[\eta\mathbf{k}^2 + i\rho\mathbf{k}\cdot\mathbf{v}_{lim}]}(\mathbf{I} - \hat{\mathbf{k}}\hat{\mathbf{k}})\rangle, \tag{4.19}$$

where brackets mean averaging over monomer coordinates $\mathbf{r}_{n,m}$. In Eq. (4.18) we explicitly highlight that the *velocity fluctuations of the tail are driven by the head part*. To consider this internal fluctuation, we neglect all the forces due to internal interactions, and assume that the force is caused by each monomer in the head part, being equal to the gravitational force $-m_0 g$.

Later, one needs to average the Oseen tensor of Eq. (4.19) over the monomer coordinates. As was shown in [59], a reasonable approximation is given by a Gaussian monomer-monomer distribution function $\Psi(\mathbf{r}_n - \mathbf{r}_m)$, with a variance corresponding to $a_0|n-m|^{\nu}$, $a$ being the segment length. Here, of course, the distribution function separates into parallel and perpendicular parts that have variances equal to $a|n-m|^{\parallel,\perp}$, respectively. The calculation of the preaveraged Oseen tensor is pretty lengthy, but straightforward. It can be shown that in the presence of the "limiting velocity field", even the pre-averaged Oseen tensor remains with non-zero off-diagonal components, which vanish if we set the limiting velocity field to zero [12, 59]. This has a consequence that the force variation in $z$ direction causes a fluctuation of the velocity field also on the $xy$ plane.

In the limit $\alpha \equiv R_\perp / R_\parallel \ll 1$, one obtains to the leading order that

$$\mathbf{H}_{nm,zz} = \frac{\log\left(|n-m|^{\nu_\parallel - \nu_\perp}\right)}{4\pi\eta a_0 |n-m|^{\nu_\parallel}} g_1(Re_{\parallel,eff}, \alpha), \tag{4.20}$$

which is the same as the zero Reynolds number result for a homogeneous rod, except that now the scaling function $g1$ is more complicated, and depends both on the ratio $\alpha$, and the effective Reynolds number $R_{\parallel,eff} = a_0|n-m|^{\nu_\parallel}$. In the $xy$ plane we found surprisingly a very different result, showing $1/R_\parallel^2$ dependence on radius of gyration, instead of the usual $1/R_{perp}$:

$$\mathbf{H}_{nm,\perp z} = \frac{\log\left(|n-m|^{\nu_\parallel - \nu_\perp}\right)}{2\pi^2\eta v_{lim} a_0^2 |n-m|^{2\nu_\parallel}} g_2(Re_{\parallel,eff}, \alpha). \tag{4.21}$$

In Eq. (4.20) and (4.21), the scaling functions $g_{1,2}$ depend on the effective Reynolds number in the $z$ direction and $\alpha$, implying that actually the previous equations hold only asymptotically in the limit $\alpha \to 0$.

Finally, the CM velocity of the polymer is obtained from Eq.(4.18) by summing over $n$ and $m$, and noticing that only the head part of the polymer contributes to forces on average. After a tedious calculation one obtains

$$\begin{aligned} \delta\mathbf{v}_{CM,tail,\parallel} &\propto \frac{N_{head}\log\left(N_{head}\right)}{4\pi\eta R_{\parallel}}; \\ \delta\mathbf{v}_{CM,tail,\perp} &\propto \frac{N_{head}\log\left(N_{head}\right)}{2\pi^2\eta R_{\parallel}^2}, \end{aligned} \tag{4.22}$$

which is the result we were after. It clearly shows that in the thermodynamic limit the fluctuations in the perpendicular direction vanish quicker than in the $z$ direction. One should realize that in thermodynamic limit the head part becomes very small compared to the tail part, and in fact also the fluctuations in the $z$ direction vanish as $1/R_{\parallel}$, as they should.

The limiting velocity of the chain $\mathbf{v}_{lim}$ is independent of the fluctuating $R_G$. Clearly the velocity fluctuations, scaling as $N_{head}/R_{\parallel}$ are smaller in magnitude compared to the limiting sedimentation velocity $\mathbf{v}_{lim} \propto N_{head}^{\beta-\nu_{\perp}}$. This means that the crossterm $2\mathbf{v}_{lim} \cdot \delta\mathbf{v}_{CM}$ gives the largest contribution to the $R_G$ dependence of the kinetic energy Eq. (4.14), being of the order

$$\begin{aligned} \frac{1}{2}M\mathbf{v}_{CM}^2 &\propto M\frac{|\mathbf{v}_{lim}|N_{head}}{R_{\parallel}} \\ &= \frac{N_{tail}N_{head}|\mathbf{v}_{lim}|}{R_{\parallel}}. \end{aligned} \tag{4.23}$$

Plugging Eq. (4.23) into Eq. (4.14), we get the free energy of the polymer chain from Eq. (4.13) as $\mathcal{F}_{total} = -k_BT\log\Psi(\mathbf{R},\mathbf{P})$, as a function of radius of gyration:

$$\begin{aligned} \mathcal{F}_{total} \propto \frac{1}{2}\frac{k}{N}\left(R_{G,\perp}^2 + R_{G,\parallel}^2\right) + \frac{1}{2}\nu\frac{N^2}{R_{G,\perp}^2 R_{G,\parallel}} \\ +\frac{1}{2}(m_0 N_{tail})\frac{|\mathbf{v}_{\rm lim}|N_{head}}{R_{G,\parallel}}. \end{aligned} \tag{4.24}$$

Here we have discarded the quadratic term in $\mathbf{v}_{\rm lim}$, being independent of $R_G$, and the logarithmic prefactor of velocity fluctuations, not giving any contribution to scaling laws. Also, we assume that in the scaling regime $N_{tail} \approx N \gg N_{head}$, such that the size of the head becomes almost independent of $N$. The equilibrium is obtained by minimizing the free energy with respect to both $R_{G,\perp}$ and $R_{G,\parallel}$ separately, and using the limiting velocity given by Eq.(4.16). The derivation is shown in Article IV, and here we mainly state the final result, which is the scaling of the parallel and perpendicular components of radius of gyration:

$$\langle R_{G,\parallel} \rangle \propto N^{(15+12\beta)/33}; \tag{4.25}$$

$$\langle R_{G,\perp} \rangle \propto N^{(7-\beta)/11}. \tag{4.26}$$

It should be noted that for a large Reynolds number, the $N$ dependence of the terminal velocity is of the form $|\mathbf{v}_{\rm lim}| \propto N^{0.05}$ using our numerical result for $\nu_\perp \approx 0.45$. In other words, in this limit the $N$ dependence of $\mathbf{v}_{\rm lim}$ becomes very weak.

### 4.2.3 Velocity Fluctuations and Effective Diffusion,

A direct consequence of the random velocity fluctuations around the steady-state limit is that in analogy to thermal systems, such fluctuations lead to the existence of finite transport coefficients [32, 34–36]. In particular, using the Green-Kubo response function formalism [16, 31] the effective diffusion coefficient for the CM of the polymer chain can be defined as in Eq. (4.2). In thermal equilibrium, the equilibrium diffusion coefficient of a polymer chain in a good solvent is known to scale as $D \propto N^{-\nu_D}$ where $\nu_D = 1$ for the Rouse model, and $\nu_D = \nu_e$ for the Zimm model. In the case of sedimenting polymer, we expect this scaling law to generalize to two independent relations as was anticipated in Eqs. (4.4).

In Fig. 4 of Article IV we show the scaling of the components of $D$ for this range of chain lengths $N \in \{16, 20, 28, 32\}$. The surprising result here is that we find for this range of values of $N$ that both diffusion coefficients actually *increase* with increasing $N$, in contrast to the thermal case. Here one should also remember that our model does not include thermal fluctuations, so we don't get the thermal limit even by setting gravitational field to zero. Best fit to the data gives $\nu_{D,\perp} = -0.22 \pm 0.11$ and $\nu_{D,\parallel} = -1.0 \pm 0.2$. From Eq. (4.18) we can calculate the magnitude of velocity fluctuations in the opposite limit to the scaling regime of radius of gyration, namely $\alpha = R_\perp \gg R_\parallel$, which is in fact true in the parameter regime of our simulations, see Fig. 4.1. The velocity fluctuation of the tail scales as

$$\begin{aligned} \delta \mathbf{v}_{CM,tail,\parallel} &= \frac{N_{head} \log\left(N_{head}\right)}{4\pi\eta R_\perp}; \\ \delta \mathbf{v}_{CM,tail,\perp} &= \frac{N_{head} \log\left(N_{head}\right)}{2\pi^2 \eta v_{lim} R_\perp^2}, \end{aligned} \tag{4.27}$$

which is the same as Eq. (4.22), but here the perpendicular component of radius of gyration is the largest dimension of the polymer, and is mainly responsible for the friction. In the same way we get a very rough approximation for diffusion coefficient of the chain, being proportional to the square of the velocity fluctuations, as

$$\begin{aligned} D_\parallel &\propto \frac{N_{head}^2}{R_{perp}^2} = N^{2(1-\nu_\perp)} \approx N^{1.1}; \\ D_\perp &\propto \frac{N_{head}^2}{R_{perp}^4} = N^{2(1-2\nu_\perp)} \approx N^{0.2}, \end{aligned} \tag{4.28}$$

where we used the numerical result $\nu_{perp} \approx 0.45$, and the approximation $N_{head} \propto N$. The empirical predictions of Eq. (4.28) give a reasonably good agreement with our numerical results. However, one should notice that these results apply only in a very limited range of $N$ values, since finally the size of the parallel component of radius of gyration exceeds the perpendicular one, indicating a transition to the scaling regime covered by Eq. (4.22). In scaling regime, it should happen that the fluctuations start to decrease, meaning that one should see a crossover in the behavior of diffusion coefficient as a function of $N$. In scaling regime the functional dependence of the velocity fluctuations in $z$ direction on radius of gyration is the same as in thermal diffusion, namely $\delta \mathbf{v}_{cm} \propto 1/R_\parallel$. However, the driving force is still the gravity $g$, and not $k_B T$ as in thermal diffusion.

## 4.3 Summary and Conclusions

In Article IV we examined the behavior of a coarse-grained polymer chain in steady state sedimentation due to gravity. Under these conditions the chain reaches a steady state, in which it continues to fluctuate irregularly through a series of configurations which include vertical and horizontal straightening and collapsing back to a globule. Despite the irregularity, it is seen that the polymer spends most of its time in the plane perpendicular to gravity. However, the shape fluctuations in the direction of gravity tend to magnify as a function of monomerization $N$, at least in the regime of simulations.

To explain these results, we developed a generalization of the Flory scaling argument for the case of steady state sedimentation. It predicts that the inertial forces induced by the head tail structure of the polymer in non-equilibrium flow alter the configuration probabilities radically.

In Sec. 4.2.2 we explained the physical mechanism driving the polymer chain into a state of asymmetric size distribution and diffusive motion. This is all caused by the convective motion in the direction of gravity, included approximately in the NS equation through the linearized convective term. Convection gives rise to increased tail fluctuations into direction of gravity, making the chain elongated. Also, it predicts a non-zero contribution from the gravitational force into motion of perpendicular component, being absent in the symmetric case. This also reveals that the diffusion coefficient scales very differently in parallel and perpendicular directions.

However, in order to quantitatively consider the asymmetry between $R_\parallel, R_\perp$ and $D_\parallel, D_\perp$ in the thermodynamic limit $N \to \infty$, an extended set of simulations is needed. In particular, it is not clear how $D$ depends on the overall sedimentation velocity of the polymer through the non-linear convective term, and how the chain conformation crossover from perpendicular plane into direction of gravity happens. Also, it would be important to verify numerically whether the velocity ansatz of Eq. (4.17) holds even qualitatively.

# 5 Summary

In this Thesis we have studied the electrostatic properties of strongly charged biomolecules, the conformations of highly stretched and charged biopolymers, and dynamics of sedimentation of long biopolymers in the presence of large amount of added electrolyte. The final statement means that in all applications the interactions between different biomolecules and ions under study have a finite range and at large distance from each other they can be considered as non-interacting.

In Sec. 2 we considered the distribution of counterions and coions around a very strongly charged surface of the biological macromolecule. Here the idea was to develop a formalism to calculate the free energy and electrostatic potential of a system composed of a few charged macromolecules, surrounded by a reservoir of oppositely charged counterions and similarly charged coions. This electrostatic potential can be used as an input to study systems in larger length scales, where the individual ion properties do not have much importance, like in DLVO theory. Both the free energy and the electrostatic potential are straightforwardly related to the ion densities of different ion types in surrounding medium. The theory developed here predicts these ion-densities in the limit of moderate or large amount of reservoir salt or electrolyte.

As an application of the electrostatic theory developed in this Thesis, we studied a benchmark case of one infinite charged wall surrounded by counterions and coions. Here we were interested in calculating also the so-called *apparent surface charge* that is equal to the total amount of charge inside a given distance from the wall, composed of the wall charge and all the charged ions inside this distance. We were able to show that under certain concentrations of added electrolyte the apparent charge changes sign from negative to positive, which is typically taken as an indication of overcharging/charge reversal. The magnitude of the integrated charge depends non-monotonically on the added electrolyte, valency of the counterions, and also ion radii. This result is in agreement with a large

number of experimental and simulation studies [38, 45–47, 69]. Also, we argue that the mechanism behind overcharging is layer formation, where the ions in the second layer behind the condensed layer stick to the ions in the layer next to the macrocharge. Our theory also predicts that the maximum of overcharging should happen at a distance of two ion-diameters from the charged wall, in accord with the previous simulation results for charged colloids [38].

In Sec. 3 we studied the statistical conformations of DNA under external stretching force. Here the interesting question is to find a relationship between the force required to produce the overstretching transition as a function of the electrolyte cooncentration. We developed a formalism that combines the one-dimensional description of the internal structure of DNA [1], i.e., hydrogen bonding, and the mesoscopic elasticity theory for the DNA-backbone [56]. The new piece of the theory is that we used a so-called global coupling between the elasticity and Ising variables, which induces the change of the elastic parameters along the overstretching transition. This coupling can be seen as a minimal model to create interaction between the different parts of the chain.

The theory predicts the force required to stretch the DNA a certain amount, i.e., the force-extension relation. We used this force-extension relation as a fitting function with unknown Ising structural parameters and renormalized separation between the charges, to be determined from fitting to the experimental data [70]. The major result is that despite of the very complicated form of the data curves, the fitting can be done with just one adjustable paramter, which turns out to be the renormalized separation between the charges. Moreover, the value of this separation varies between the structural separation and Bjerrum length, in qualitative agreement with Manning condensation theory. We also showed that other fitting parameters have barely any salt dependence, and for the given data they can be taken as constants. This also demonstrates that the necessary electrostatic interactions are mediated via elasticity, and there is no need to introduce any other terms into the free energy.

Finally Sec. 4 considered the sedimentation dynamics of very long biopolymers, such as DNA, under the gravitational field. Here we developed an effective theory to take into account non-zero Reynolds number contributions to the sedimentation velocity, to the size and the shape, and to the diffusion coefficient of the polymer. The theory is based on the hypothesis that the velocity of the sedimenting polymer can be divided into two parts, consisting of the average sedimentation velocity and fluctuations described by linearized NS equations. Furthermore, we took into account the convection of the velocity in the direction opposite to the sedimentation by linearized convective term. However, all the nonlinearities are assumed to be described by the average sedimentation velocity, being given by the empirical formula fitted from experiments. The theoretical model was compared to the simulation data in Article IV giving very good agreement in the regime of simulation parameters.

The main results here are that the polymer is driven to a non-equilibrium steady-state, where it keeps on fluctuating between vertically fully elongated and compacted conformations. The velocity fluctuations are mainly due to this internal motion of polymer, and seem to be magnifying as a function of monomerization in the regime of simulations. We argue theoretically that for longer polymers the chain should go through a crossover from horizontal configuration into elongated one, suct that finally the chain is fully elongated, and the horizontal head part of the polymer vanishes. From the dynamical point of view, this shows up in the velocity fluctuations that first keep on increasing up to the crossover, after which they start to decrease when the length of the chain is increased further. It is remarkable that the scaling theory developed here predicts the chain properties on both sides of the crossover.

# References

[1] A. Ahsan, J. Rudnick, and R. Bruinsma. 1998. Elasticity Theory of the B-DNA to S-DNA Transition. Biophys. J. 74, pages 132–137.

[2] B. Alberts, D. Bray, J. Lewis, M. Raff, K. Roberts, and J. D. Watson. 1994. Molecular Biology of the Cell. Garland Publishing, New York, 3rd edition.

[3] C. G. Baumann, S. B. Smith, V. A. Bloomfield, and C. Bustamante. 1997. Ionic Effects on the Elasticity of Single DNA Molecules. Proc. Natl. Acad. Sci. USA 94, pages 6185–6190.

[4] M. Le Bret and B. Zimm. 1984. Distribution of counterions around a cylindrical polyelectrolyte and Manning's condensation theory. Biopolymers 23, page 287.

[5] Y. Burak and D. Andelman. 2001. Discrete aqueous solvent effects and possible attractive forces. J. Chem. Phys. 114, pages 3271–3283.

[6] C. R. Calladine and Drew Horace. 1992. Understanding DNA. Academic Press INC., San Diego.

[7] R. Clark and C. Lange. 1980. A quantitative test of Zimm's model for the rotor-speed-department sedimentation of linear DNA-moelcule. Biopolymers 19, pages 945–964.

[8] H. Clausen-Schaumann, M. Rief, R Krautbauer, and H. E. Gaub. 2000. Force spectroscopy with single bio-molecules. J. Comp. Chem. 4, pages 524–530.

[9] H. Clausen-Schaumann, M. Rief, C. Tolksdorf, and H. E. Gaub. 2000. Mechanical stability of single DNA molecules. Biophys. Chem. 78, pages 1997–2007.

[10] P. Cluzel, A. Lebrun, R. Lavery, J-L. Viovy, D. Chatenay, and F. Caron. 1996. DNA: An extensible molecule. Science 271, pages 792–794.

[11] P. Dai, Y. Mu, L. Nordenskiold, and J. R. C. van der Maalen. 2008. Molecular Dynamics Simulation of Multivalent-Ion Mediated Attraction between DNA Molecules. Phys. Rev. Lett. 100, page 118301.

[12] M. Doi and S. F. Edwards. 1986. The Theory of Polymer Dynamics. Oxford science publications, Oxford.

[13] S. F. Edwards and A. Lenard. 1962. Exact Statistical Mechanics of a One-Dimensional System with Coulomb Forces. II.The Method of Functional Integration. J. Math. Phys. 3, pages 778–792.

[14] R. P. Feynman and A. R. Hibbs. 1965. Quantum Mechanics and Path Integrals. McGraw-Hill, New York.

[15] P. J. Flory. 1940. Molecular Size Distribution in Ethylene Oxide Polymer. J. Am. Chem. Soc. 62, page 1561.

[16] R. Gomer. 1990. Diffusion of adsorbates on metal surfaces. Rep. Prog. Phys. 53, page 917.

[17] Niels Gronbech-Jensen, R. J. Mashl, and R. F. Bruinsma. 1997. Counterion-Induced Attraction between Rigid Polyelectrolytes. Phys. Rev. Lett. 78, pages 2477–2480.

[18] A. Grosberg and A. Khoklov. 1994. Statistical Physics of Macromolecules. AIP Press, New York.

[19] L. Gulbrand, B. Jonsson, H. Wennerstrom, and P. Linse. 1984. Electrical Double Layer Forces. A Monte Carlo Study. J. Chem. Phys. 80, pages 2221–2228.

[20] A. Hanke, M. G. Ochoa, and R. Metzler. 2008. Denaturation transition of stretched DNA. Phys. Rev. Lett. 100, pages 018106–1–4.

[21] J.-P. Hansen and I. R. McDonald. 1986. Theory of Simple Liquids. Academic Press, London, 2nd edition.

[22] P. L. Hansen and R. Podgornik. 2001. Wormlike chains in the large-$\mathrm{d}$ limit. J. Chem. Phys. 114, pages 8637–8648.

[23] P. L. Hansen, R. Podgornik, and V. A. Parsegian. 2001. Osmotic Properties of DNA: Critical Evaluation of Counterion Condensation Theory. Phys. Rev. E 64, pages 021907–1–4.

[24] S. E. Harding. 1993. Analytical Ultracentrifugation in Biochemistry and Polymer Science. Royal Soc. Chem., Cambridge.

[25] J. D. Jackson. 1999. Classical Electrodynamics. John Wiley & Sons, New York.

[26] P. Kekicheff, S. Marcelja, T.J. Senden, and V. E. Shubin. 1993. Charge reversal seen in electrical double layer interaction of surfaces immersed in 2:1 calcium electrolyte. J. Chem. Phys. 99, page 6098.

[27] R. Kjellander and S. Marcelja. 1989. A theoretical and experimental study of forces between charged mica surfaces in aqueous $CaCl_2$ solutions. J. Chem. Phys. 92, pages 4399–4407.

[28] R. Kjellander, S. Marcelja, and J. P. Quirk. 1988. Attractive double-layer interactions between calcium clay particles. J. Colloid Interface Sci. 126, page 194.

[29] M. W. Konrad and J. I. Bolonick. 1996. Molecular dynamics simulation of DNA stretching is consistent with the tension observed for extensions and strand separation and predicts a novel ladder structure. J. Am. Chem. Soc. 118, pages 10989–10994.

[30] Krautbauer and al. 2000. Denaturation. Angew. Chemie. Int. Edit. 39, pages 3912–3920.

[31] R. Kubo. 1957. Statistical-Mechanical Theory of Irreversible Processes. I. General Theory and Simple Applications to Magnetic and Conduction Problems. J. Phys. Soc. Jpn. 12, page 570.

[32] E. Kuusela. 2005. Steady-State Sedimentation of Non-Brownian Particles with Finite Reynolds Number. Otamedia Oy, Espoo.

[33] E. Kuusela, K. Hofler, and S. Schwarzer. 2001. Simulation of settling speed and orientation distribution insuspensions of prolate spheroids. J. Eng. Math. 41, page 221.

[34] E. Kuusela, J. M. Lahtinen, and T. Ala-Nissila. 2003. Collective Effects in Settling of Spheroids under Steady-State Sedimentation. Phys. Rev. E 90, page 094502.

[35] E. Kuusela, J. M. Lahtinen, and T. Ala-Nissila. 2004. Origin of non-Gaussian velocity distributions in steady-state sedimentation. Europhys. Lett. 65, page 13.

[36] E. Kuusela, J. M. Lahtinen, and T. Ala-Nissila. 2004. Sedimentation dynamics of spherical particles in confined geometries. Phys. Rev. E 69, page 066310.

[37] A. Lebrun and R. Lavery. 1996. Modelling extreme stretching of DNA. Nature 24, pages 2260–2267.

[38] O. Lenz and C. Holm. 2007. Simulation of Charge Reversal in Salty Environmeents: Giant overcharging? Eur. Phys. J. E 26, pages 191–195.

[39] J. Levin. 1996. Modelling extreme stretching of DNA. Nature 24, pages 2260–2267.

[40] R. Lipowsky, R. Sackmann, and E. Eds. 1995. Handbook of Biological Physics. Elsevier Science, Amsterdam.

[41] A. P. Lyubartsev and L. Nordenskiold. 1995. A Monte Carlo simulation study of ion distribution and osmotic pressure in hexagonally oriented DNA. J. Phys. Chem. B 99, pages 10373–10382.

[42] G. S. Manning. 1969. Limiting laws and counterion condensation in polyelectrolyte solutions I. Colligative properties. J. Chem. Phys. 51, pages 924–933.

[43] J. Marra. 1986. Direct Measurement of The Interaction between Phosphatidylglycerol Bilayers in Aqueous Electrolyte Solutions. Biophys. J. 50, pages 815–825.

[44] Harold Mcgee. 1984. "Milk and Dairy Products". On Food and Cooking: The Science and Lore of the Kitchen.". Charles Scribner's Sons, New York.

[45] R. Messina, C. Holm, and K. Kremer. 2000. Ground state of the unlike charged colloids: An analogy with ionic bonding. Europhys. Lett. 51, pages 461–467.

[46] R. Messina, C. Holm, and K. Kremer. 2000. Strong Attraction between Charged Spheres due to Metastable Ionized States. Phys. Rev. Lett. 85, pages 872–875.

[47] R. Messina, C. Holm, and K. Kremer. 2001. Strong electrostatic interactions in spherical colloidal systems. Phys. Rev. E 64, pages 021405–1–4.

[48] A. Moreira and R. R. Netz. 2000. Strong-coupling theory for counter-ion distributions. Europhys. Lett. 52, pages 705–711.

[49] A. Moreira and R. R. Netz. 2002. Counterions at charge-modulated substrates. Europhys. Lett. 57, pages 911–917.

[50] A. Naji and R. R. Netz. 2004. Attraction of Like-Charged Macroions in the Strong-Coupling Limit. Europhys. Lett. 13, pages 43–59.

[51] R. R. Netz. 2001. Electrostatics of counter-ions at and between planar charged walls: From Poisson-Boltzman to the strong-coupling theory. Europhys. Lett. 5, pages 557–574.

[52] R. R. Netz and H. Orland. 1999. Beyond Poisson-Boltzman: Fluctuation effects and correlation functions. Eur. Phys. J. E 1, pages 203–214.

[53] Roland R. Netz. 2001. Strongly Stretched Semiflexible Extensible Polyelectrolytes and DNA. Macromolecules 34, pages 7522–7529.

[54] Th. Odijk. 1995. Poisson-Boltzman-Donnan theory. Macromolecules 28, page 7016.

[55] R. Podgornik. 1989. An analytical treatment of the first-order correction to the Poisson-Boltzmann interaction free energy in the case of counterion-only Coulomb fluid. J. Phys. A: Math. Gen. 23, pages 275–284.

[56] R. Podgornik, P. L. Hansen, and V. A. Parsegian. 2000. Elastic Moduli Renormalization in Self-interacting Stretchable Polyelectrolytes. J. Chem. Phys. 113, pages 9943–9950.

[57] R. Podgornik and B. Zeks. 1988. Inhomogeneous Coulomb Fluid. J. Chem. Soc. Faraday Trans 84, pages 611–631.

[58] O. Punkkinen. 2009. To be submitted. Phys. Rev. E .

[59] O. Punkkinen, E. Falck, and I. Vattulainen. 2005. Dynamics and Scaling of Polymers in a Dilute Solution: Analytical Treatment in Two and Higher Dimensions. J. Chem. Phys. 122, page 094904.

[60] O. Punkkinen, A. Naji, R. Podgornik, I. Vattulainen, and P.-L.Hansen. 2008. Ionic Cloud Distribution Close to a Charged Surface in the Presence of Salt. Europhys. Lett. 82, page 48001.

[61] O. Punkkinen, I. Vattulainen, P. L. Hansen, and R. Podgornik. 2009. Counter- and Coion Distributions Close to a Strongly Charged Surface in the Limit of Weakly Coupled Bulk Salt. HIP-2009-12/TH .

[62] I. Rouzina and V. A. Bloomfield. 1996. Macroion Attraction Due to Electrostatic Correlation Between Screening Counterions, 1.Mobile Surface-Adsorbed Ions and Diffuse Ion Cloud. J. Chem. Phys. 100, pages 9977–9989.

[63] I. Rouzina and V. A. Bloomfield. 2001. Force-induced melting of the DNA double helix 1.Thermodynamic analysis. Biophys. J. 80, pages 882–893.

[64] I. Rouzina and V. A. Bloomfield. 2001. Force-induced melting of the DNA double helix 2.Effect of solution conditions. Biophys. J. 80, pages 894–900.

[65] I. Rubenstein and S. B. Leighton. 1974. The influence of rotor speed on the sedimentation behavior in sucrose gradients of high molecular weight DNA's. Biophys. Chem. 1, pages 292–299.

[66] X. Schlagberger and R. R. Netz. 2007. Anomalous Sedimentation of Polymer Far from Equilibrium. Phys. Rev. Lett. 98, pages 128301–128304.

[67] B. I. Shklovskii. 1999. Screening of a macroion by multivalent ions: Correlation-induced inversion of charge. Phys. Rev. E 60, page 5802.

[68] S. B. Smith, Y. J. Cui, and C. Bustamante. 1996. Overstretching B-DNA:The elastic response of individual double-stranded and single-stranded DNA molecules. Science 271, pages 795–799.

[69] M. Trulsson, Bo Jönsson, T. Åkesson, and J. Forsman. 2007. Repulsion between Oppositely Charged Macromolecules or Particles. Langmuir 23, pages 11562–11569.

[70] J. R. Wenner, M. C. Williams, I. Rouzina, and V. A. Bloomfield. 2002. Salt Dependence of the Elasticity and Overstretching Transition of Single DNA Molecules. Biophys. J. 82, pages 3160–3169.

[71] H. Wennerström, A. Khan, and B. Lindman. 1991. Ionic surfactants with divalent counterions. Adv. Coll. Int. Sci. 34, page 433.

[72] F. M. White. 1991. Viscous Fluid Flow. McGraw-Hill Book Co., Singapore.

[73] M. C. Wiliams and I. Rouzina. 2002. Force spectroscopy of single DNA and RNA molecules. Curr. Opin. Struct. Biol. 12, pages 330–336.

[74] M. C. Williams, I. Rouzina, and V. A. Bloomfield. 2001. The effect of pH on the overstretching transition of dsDNA: evidence of force-induced DNA melting. Biophys. J. 80, pages 874–882.

[75] M. C. Williams, I. Rouzina, and V. A. Bloomfield. 2001. Entropy and heat capacity of DNA melting from temperature dependence of single molecule stretching. Biophys. J. 80, pages 1932–1939.

[76] B. H. Zimm. 1956. Dynamics of Polymer Molecules in Dilute Solution: Viscoelasticity, Flow Birefringence and Dielectric Loss. J. Chem. Phys. 24, page 269.

ISBN 978-951-22-9915-7
ISBN 978-951-22-9917-1 (PDF)
ISSN 1795-2239
ISSN 1795-4584 (PDF)